Author Manuscript

Author Manuscript

Author Manuscript

Author Manuscript

HHS Public Access

Author manuscript

Dev Cell. Author manuscript; available in PMC 2025 January 08.

Published in final edited form as:

Dev Cell. 2024 January 08; 59(1): 20–32.e6. doi:10.1016/j.devcel.2023.11.015.

Sweat gland development requires an eccrine dermal niche and couples two epidermal programs

Heather L. Dingwall[1], **Reiko R. Tomizawa**[1], **Adam Aharoni**[1], **Peng Hu**[1,2], **Qi Qiu**[1], **Blerina Kokalari**[1], **Serenity M. Martinez**[1], **Joan C. Donahue**[1], **Daniel Aldea**[1], **Meryl Mendoza**[1], **Ian A. Glass**[3], **Birth Defects Research Laboratory (BDRL)**[3,4], **Hao Wu**[1], **Yana G. Kamberov**[1,*]

[1]Dept. of Genetics, Perelman School of Medicine, Philadelphia, PA, USA

[2]Present address: College Fisheries and Life Sciences, Shanghai Ocean University, Shanghai, China

[3]Dept. of Pediatrics, University of Washington, Seattle, WA, USA

[4]Seattle Children's Research Institute, University of Washington, Seattle, WA, USA

SUMMARY

Eccrine sweat glands are indispensable for human thermoregulation and like other mammalian skin appendages form from multipotent epidermal progenitors. Limited understanding of how epidermal progenitors specialize to form these vital organs has precluded therapeutic efforts towards their regeneration. Herein, we applied single nucleus transcriptomics to compare the expression content of wildtype, eccrine-forming mouse skin to that of mice harboring a skin-specific disruption of *Engrailed 1 (En1)*, a transcription factor that promotes eccrine gland formation in humans and mice. We identify two concurrent, but disproportionate, epidermal transcriptomes in the early eccrine anlagen: one that is shared with hair follicles, and one that is *En1*-dependent and eccrine-specific. We demonstrate that eccrine development requires the induction of a dermal niche proximal to each developing gland in humans and mice. Our study defines the signatures of eccrine identity and uncovers the eccrine dermal niche, setting the stage for targeted regeneration and comprehensive skin repair.

Graphical Abstract

*Correspondence: yana2@pennmedicine.upenn.edu.
Lead Contact: yana2@pennmedicine.upenn.edu

AUTHOR CONTRIBUTIONS

YGK conceived of and supervised the study. YGK and HLD designed the experiments and wrote the manuscript. HLD, RRT, AA, BK, PH, QQ, SMM, JCD, DA, and MM performed the experiments. HLD and YGK analyzed and interpreted the data. HW, IAG, the BDRL and YGK contributed resources and acquired funding to support the study.

Publisher's Disclaimer: This is a PDF file of an unedited manuscript that has been accepted for publication. As a service to our customers we are providing this early version of the manuscript. The manuscript will undergo copyediting, typesetting, and review of the resulting proof before it is published in its final form. Please note that during the production process errors may be discovered which could affect the content, and all legal disclaimers that apply to the journal pertain.

DECLARATION OF INTERESTS

The authors declare no competing interests.

Author Manuscript Author Manuscript Author Manuscript Author Manuscript

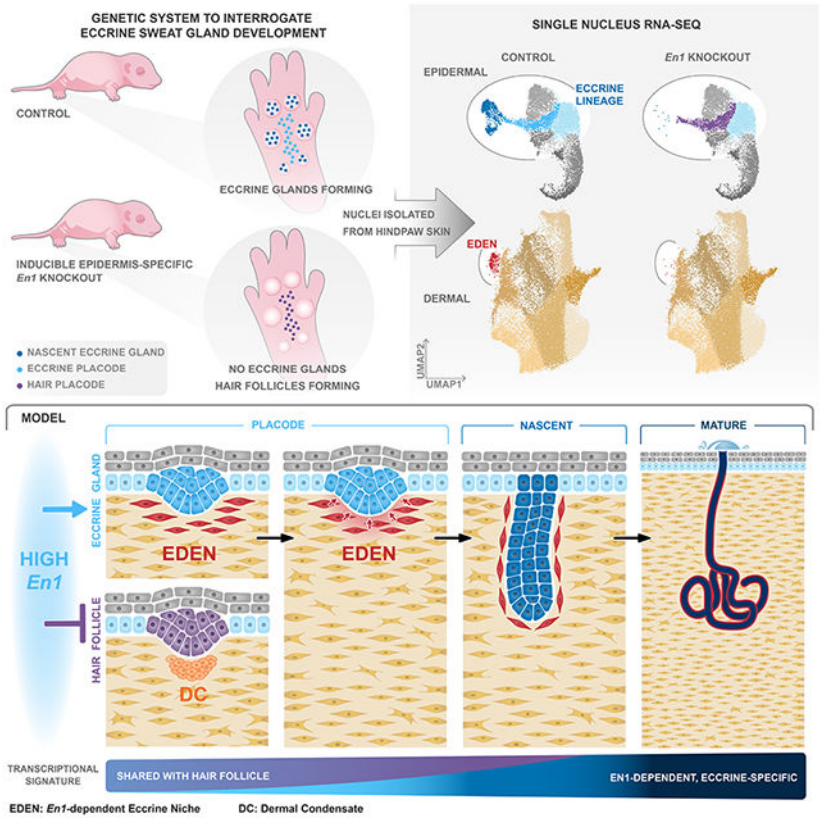

eTOC

Dingwall *et al.* demonstrate that the development of eccrine sweat glands, the major effector of the human thermoregulatory system, requires the induction of EDEN, an evolutionarily conserved dermal niche, and couples two concurrent but separable transcriptomes. These findings resolve the molecular signatures and cellular drivers of eccrine identity.

Keywords

Eccrine gland; sweat; ectodermal appendage; skin appendage; development; dermal niche

Introduction

Eccrine sweat glands are the most numerous appendage found in human skin and are critically important for human thermoregulation, removing excess heat and protecting our bodies from lethal overheating[1-3]. Despite their importance, there are no therapeutic paradigms to regenerate eccrine glands for reconstructive skin repair, leaving patients with epithelial injuries such as extensive burns with extreme, even life-threatening deficits in thermoregulation[1,2,4-7]. Thwarting these efforts is a lack of information on how the skin forms these critical appendages in the first place.

Eccrine glands belong to the ectodermal appendage organ class, which also includes hair follicles and mammary glands[2,8]. These organs form from thickenings of the deepest (basal)

Author Manuscript Author Manuscript Author Manuscript Author Manuscript

layer of the epidermis called placodes, and mature by growing down and differentiating into the underlying connective tissue dermis[8-11]. To date, studies investigating eccrine gland development have largely implicated molecular regulators and developmental pathways shown to also be required for the formation of other ectodermal appendages, like hair follicles and mammary glands[5,8,10,12-18]. However, the molecular factors that distinguish epidermal progenitors as they transition through eccrine gland development are poorly understood[5,8,10,12,19,20].

For other ectodermal appendages such as hair follicles, teeth, and mammary glands, a major function of the placode is to induce local condensation of the underlying dermis to form a specialized niche that engages in coordinated and reciprocal interaction with the appendage progenitors to direct further development[3,33-37]. Strikingly, eccrine gland placodes, and indeed developing eccrine glands at any stage, are not associated with the morphologically-evident mesenchymal condensations that are the hallmarks of known dermal niches and an analogous niche for the eccrine gland has not been identified[23,31]. Accordingly, it is unknown if eccrine developmental progression requires extrinsic input from the dermis or diverges from the classical ectodermal appendage paradigm[8,10,12,21-25].

To enable precise targeting of the eccrine gland developmental program, we took advantage of an *in vivo* system that allows direct comparison within the same spatiotemporal context between the developmental program for eccrine glands and that of another major ectodermal appendage, the hair follicle. Specifically, we capitalized on the fact that in the eccrine-forming skin of mice, the palmar/plantar (volar) paw, expression of the *Engrailed 1* (*En1*) gene promotes the formation of eccrine glands and concomitantly inhibits the formation of hair follicles[5,12,19,26-28]. Using genetic modulation of *En1* levels in this tissue, we shifted the composition of mouse volar skin from eccrine to hair-forming and applied single nucleus transcriptomics to parse out the transcriptional and cellular identifiers that make the developing eccrine gland distinct.

Results

Targeted disruption of eccrine development by inhibition of eccrine placode identity

En1 is expressed throughout the deepest (basal) layer of the epidermis in the palmar/plantar (volar) skin of the mouse paw and is focally upregulated in the earliest eccrine anlagen, or placodes, that form therein[12,19,29]. This expression pattern is recapitulated in human fetal skin in regions where eccrine glands are developing[12,28]. Importantly, the level of epidermal *En1* during the developmental period when eccrine placodes are specified is directly correlated with the number of eccrine glands that form in mouse and human skin, and reducing *En1* levels results in a dosage-dependent decrease in the number of eccrine glands[5,12,19,27,28,30]. We therefore reasoned that disrupting epidermal *En1* expression at the eccrine placode stage would lead to a specific depletion of the eccrine developmental signature from the skin.

To this end, we derived doxycycline inducible, epidermis-specific, *En1* null, or knock-out, mice (En1-cKO) by breeding mice harboring alleles for a tetracycline responsive Cre recombinase (tetO-Cre); a basal keratinocyte-specific reverse tetracycline transactivator

Author Manuscript Author Manuscript Author Manuscript Author Manuscript

(Krt5-rtTA); and a conditional *En1* null allele (*En1*^{flox})[31-33]. We induced *En1* disruption in the Keratin 5 (Krt5)-positive, basal epidermis by administering doxycycline to pregnant dams on embryonic day (E) 16.5 (Figure 1A). At this developmental stage the first eccrine placodes are forming in the six thickened elevations, or footpads, located at the periphery of the volar hindpaw [10-12,19]. On postnatal day (P) 2.5, we harvested the volar skin from En1-cKO (tetO-Cre/+;Krt5-rtTA/+;En1$^{flox/flox}$) and Control animals (En1$^{flox/flox}$, Krt5-rtTA/+;En1$^{flox/flox}$, and tetO-Cre/+;En1$^{flox/flox}$) and compared their volar appendage compositions. Consistent with our previous findings in wildtype mice, developing eccrine glands at multiple stages are simultaneously present in P2.5 Control volar skin[19]. In the footpads, where eccrine gland development began days earlier, nascent-stage eccrine glands that are co-positive for the pan-appendage marker EDAR and for *En1* expression, are differentiating and proliferating into the underlying dermis (Figure 1B)[11,19]. Importantly, the centrally-located interfootpad volar skin of Control mice is populated by placode-stage eccrine glands that show characteristic upregulation of *En1* and are also positive for EDAR (Figure 1B-bottom left)[10,11,19]. In contrast, the footpads and the interfootpad regions of P2.5 En1-cKO mice are significantly depleted of nascent eccrine glands and eccrine placodes, respectively (Figure 1B right panels). Moreover, we find that the interfootpad regions of En1-cKO mice are populated by hair follicle placodes (Figure 1B, bottom-right). Each hair follicle placode is readily differentiated from its eccrine counterparts by an underlying dermal condensate (DC), a morphologically evident aggregate of dermal cells that is the instructive niche for each developing hair follicle and the precursor of the dermal papilla (Figure 1B, bottom-right, arrowheads indicate DC)[8,21,22,22-25].

Analyses of adult Control and En1-cKO mice confirm that the regimen we used to disrupt epidermal *En1* during development permanently inhibits eccrine formation (Figure S1A). We find that compared to Controls, the volar skin of adult En1-cKO mice exhibits a dramatic reduction in footpad eccrine glands coupled with a near-complete loss of these organs in the interfootpad space, as well as an increase in the number of fully formed, interfootpad hair follicles (Figure S1B-E; Tables S1-S3).

Our findings demonstrate that genetic manipulation of the *En1* locus in the basal epidermis can be used as a tool to specifically perturb the eccrine developmental program at its onset. Collectively, the reciprocal effect of *En1* on P2.5 eccrine and hair placode identities in the interfootpad space, and the loss of differentiating nascent eccrine glands in the footpads of En1-cKO mice at this stage, makes this an ideal experimental system to capture not only the eccrine developmental program but also the transitions that characterize its progression (Figure 1C).

Single nucleus RNA-sequencing recovers transcriptional signatures of the primary skin layers

The volar hindpaw skin of P2.5 mice is composed of many different cell types, which have differential sensitivity to *En1* and varying degrees of involvement in eccrine gland development. Accordingly, we adapted Drop-seq-based, single nucleus RNA-sequencing (snRNA-seq) to recover the transcriptional profiles of P2.5 Control and En1-cKO skin samples[34-36]. Using the regimen described above, we dosed pregnant dams with doxycycline

Author Manuscript Author Manuscript Author Manuscript Author Manuscript

at E16.5 and collected the volar hindpaw skin of P2.5 Control and En1-cKO pups for snRNA-seq (Figure 1A, C). For each of the three profiled genotypes (two Control genotypes: $En1^{flox/flox}$, Krt5-rtTA/+; $En1^{flox/flox}$; one En1-cKO genotype: tetO-Cre/+;Krt5-rtTA/+;$En1^{flox/flox}$), we profiled two biological replicates, where each replicate was comprised of pooled, volar hindpaw skins from five mice of the same genotype. In total, the transcriptomes of 45,370 sequenced nuclei passed quality control filtering and were interrogated in subsequent analyses.

After sample integration with Harmony, initial clustering on the merged data from all nuclei across Control and En1-cKO groups yielded 23 clusters (Figure 1D; Figure S2A)[37]. Sample replicates showed substantial overlap both via principal components analysis and upon further dimensionality reduction via UMAP (Figure S2B). Analysis for marker gene enrichment reveals that our experiment captured the transcriptomes of nuclei from the two major compartments of the skin, namely nuclei of epidermal (blue) origin and of dermal (yellow) origin (Figure 1D, E; Figure S2C, D and Data S1A). Characteristic of the epidermal skin layer, we find clusters that show enrichment for the epidermal makers *Cdh1* (e-cadherin), *Cdh3* (p-cadherin), and *Trp63* (p63) (9,070 nuclei; Figure 1E and Figure S2C, Data S1A)[38-40]. The two Control genotypes contribute 6013 nuclei to the epidermal clusters, while the En1-cKO genotype contributes 3057 nuclei. Nuclei from clusters of a nominally dermal origin, which are the most abundant populations captured in our analyses, express known fibroblast markers including *Pdgfr alpha* (*Pdgrfa*), *Cd44*, and *Collagen type I alpha 2 (Col1a2*) (25,859 nuclei; Figure 1E, Figure S2D and Data S1A)[41]. Of these, the two Control genotypes contribute 17,398 nuclei to the dermal clusters, and the En1-cKO genotype contributes 8461 nuclei. Based on marker enrichment, we additionally identify clusters of endothelial, smooth muscle, and immune origins (Figure 1D gray, Figure S2E, F and Data S1A). These findings demonstrate that the nuclear transcriptome reflects the cellular heterogeneity of the volar skin and that our dataset captures expression profiles from the primary skin populations from both Control and En1-cKO experimental samples.

A specialized transcriptome dominates the expression landscape of nascent stage eccrine glands

Like all ectodermal appendages, eccrine glands form from *Krt5* and *Krt14*-expressing basal keratinocytes[8-12]. All cells of the developing eccrine gland retain expression of these basal-specific epidermal markers from the placode stage through the nascent period[9,11]. We observe enrichment for *Krt5* and *Krt14* in clusters 2, 10, 14, and 15, suggesting that the expression signatures of eccrine epidermal progenitors are likely to be contained within this subset of clusters (Figure 2A and Data S1A). Consistent with this, we find that cluster 14 is almost entirely depleted of En1-cKO nuclei, accounting for just 1.64% of En1-cKO epidermal nuclei in the dataset but accounting for 17.71% of epidermal nuclei recovered from Controls (Figure 2B, C). *In situ* hybridization to detect *Trpv6* and other top marker genes of cluster 14 reveals a consistent pattern of enrichment in nascent eccrine glands in the hindpaw footpads of wildtype mice (Figure 2D, E; Figure S3A, B). That the nascent gland transcriptome is sufficiently diverged as to cluster separately from the other epidermal populations shows that at this stage of development, the overriding transcriptional character

Author Manuscript Author Manuscript Author Manuscript Author Manuscript

of eccrine epidermal progenitors is highly specialized and differentiated with respect to the rest of the epidermis.

Identification of an eccrine developmental lineage in the epidermis

We specifically interrogated the heterogeneity of the epidermal clusters with a goal of resolving finer scale expression differences and identifying transcriptional signatures of pre-nascent stage eccrine gland progenitors including those of the eccrine placodes. After clustering only the epidermal nuclei isolated from merged Control and En1-cKO genotypes, we find that these further resolve into nine epidermal subclusters (Epi0-8) (Figure 2F; Data S1B). Of these, Epi5 and Epi8 correspond to the validated nascent gland cluster 14 in the initial analysis, while nuclei in Epi2, Epi6, and Epi7 are characterized by enrichment for the suprabasal markers *Krt1* and *Krt10* (Figure S3C, D; Data S1B)[9,11]. Since early eccrine epidermal progenitors, including those of the placode, are basal in character, the nuclei within Epi0, Epi1, Epi3, or Epi4, which are enriched for the basal epidermal markers *Krt5* and *Krt14*, may represent these earlier stages of eccrine gland development (Figure S3C-E; Data S1B).

Trajectory inference performed on all epidermal nuclei identifies a lineage that originates with cluster Epi0, which bears the transcriptional hallmarks of multi-potent basal epidermal keratinocytes, and ends with the validated nascent eccrine gland clusters Epi5 and Epi8 (Figure 2G; Figure S3D; Data S1B). Epi3 represents an intermediate state along this inferred lineage and is enriched for transcripts involved in ectodermal appendage development including *Edar* (Figure S3D-F; Data S1B).

To classify the Epi3 nuclei, we investigated the expression of *Lgr6*, which is the top upregulated transcript of this subcluster compared to all other epidermal populations (Figure 2H; Figure S3D; Data S1B). *Lgr6* is known to be expressed in hair follicle placodes, suggesting that Epi3 may capture the transcriptional signatures of the earliest appendage primordia[56]. Consistent with this, we find that in the volar hindpaw skin of P2.5 *Lgr6-EGFP* knock-in reporter mice, EGFP is expressed in the eccrine placodes of the interfootpad space and in the nascent glands of the footpads (Figure 2H, I; Data S1B). These collective data reveal that our snRNA-seq dataset captures a continuous eccrine developmental lineage. Notably, both Control and En1-cKO nuclei contribute to the early inferred eccrine lineage in the epidermis, and Control and En1-cKO samples cluster together in Epi0 and the early portion of Epi3, the origin and intermediate phases of the lineage, respectively (Figure 2J; Figure S3F). These observations suggest that during the initial stages of eccrine development, including during the placode stage, the transcriptional identity of eccrine progenitors is highly concordant with that of early hair follicle progenitors.

An *Engrailed 1*-dependent transcriptome distinguishes the sweat gland placode from that of the hair follicle

Our findings reveal that nuclei derived from placode-stage volar appendages, both eccrine gland and hair follicle, are represented in Epi3. We reasoned that the transcriptional signature of the eccrine placode could be resolved by specifically comparing the transcriptional content of Control (eccrine forming) versus En1-cKO (hair forming) nuclei

Author Manuscript Author Manuscript Author Manuscript Author Manuscript

within this intermediate cluster. We compared pseudo-bulk expression profiles of nuclei from Epi3 for Control versus En1-cKO samples (Figure 2K). This analysis identifies only 29 transcripts that are significantly differentially expressed between the Epi3 nuclei derived from the two conditions (Likelihood Ratio Test: adjusted $p < 0.01$; log2 fold change > 0.58). Of these, nine are relatively upregulated in the Control (eccrine) samples compared to the En1-cKO (hair) samples (Figure 2K).

Our targeted comparative analysis identified the secreted Wnt inhibitor *Dkk4* as a nuclear transcript that is relatively enriched in the eccrine-containing Controls versus En1-cKO samples (Figure 2K). *Dkk4* expression has previously been reported in placode stage hair follicles and eccrine glands, which we confirmed by *in situ* hybridization in P2.5 volar skin of wildtype mice (Figure S3G)[10,42-45]. To validate the quantitative enrichment of *Dkk4* in eccrine placodes relative to hair follicle placodes, we took advantage of strain specific differences in the number of volar hair follicles and eccrine glands between C57BL/6N and FVB/N mice[19]. We have previously reported that, on average, the hindpaw interfootpad region of FVB/N mice contains 39 eccrine glands and 5 hair follicles, while the same region in C57BL/6N mice contains 8 eccrine glands and 65 hair follicles[19]. Using genetic mapping, we have previously implicated the higher expression of epidermal *En1* in FVB/N P2.5 volar hindpaw skin as the major causal driver for the specification of more eccrine gland placodes and fewer hair follicles placodes in this strain versus the P2.5 volar skin of C57BL/6N mice[19]. Analysis of *Dkk4* expression by qRT-PCR in P2.5 FVB/N and C57BL/6N volar hindpaws reveals a significant upregulation of *Dkk4* in the predominantly eccrine placode-containing skin of FVB/Ns relative to that of C57BL/6N (Figure 2L; Mann-Whitney-Wilcoxon test, *Dkk4:* $p = 0.0495$, $Z = -1.964$, $r = -0.8$). Notably, the effect size estimate of *Dkk4* upregulation is equivalent to that of *En1* upregulation in FVB/N as compared to C57BL/6N (Figure 2L; Mann-Whitney-Wilcoxon test, *En1*: $p = 0.0495$, $Z = -1.964$, $r = -0.8$).

The relative increase of *Dkk4* expression in eccrine gland versus hair follicle placodes confirms the existence of a specific signature of eccrine identity that is dependent on the epidermal expression of *En1*. Taking into account the extensive transcriptional similarity we observe for Control and En1-cKO nuclei early in the inferred eccrine epidermal lineage, our data are consistent with the concurrent but disproportionate representation of two distinct transcriptional programs in the eccrine placode: a major transcriptome that is shared with the hair follicle placode; and a relatively underrepresented transcriptome that distinguishes the eccrine placode and is associated with its identity.

Identification of an eccrine-associated dermal lineage

Skin-specific disruption of *En1* not only depletes eccrine-associated epidermal populations, but also results in dramatic depletion of En1-cKO nuclei from primary cluster 20, which is of dermal rather than epidermal origin (Figure 1D, Figure 3A). Nuclei from cluster 20 account for 1.99% and 0.08% of Control and En1-cKO dermal populations, respectively (Figure 3B). *S100a4* is the top marker gene that differentiates cluster 20 from all other dermal populations (Figure 3C; Figure S2D; Data S1C). Using *in situ* hybridization, we find that *S100a4* is specifically expressed in PDGFRA-positive dermal fibroblasts immediately

Author Manuscript Author Manuscript Author Manuscript Author Manuscript

surrounding the nascent stage eccrine glands in the footpads of P2.5 wildtype mice (Figure 3D). This pattern is recapitulated by *Tnc*, another top marker of cluster 20 (Figure S4A, B; Figure S2D; Data S1C). The presence of a dermal sheath around nascent stage eccrine glands of mice was previously observed histologically by Cui and colleagues[10]. Consistent with the specific association of the cluster 20 transcriptional signature with dermal cells that surround the nascent glands, we find that *S100a4* expression is lost in the footpads of En1-cKO mice at P2.5 (Figure 3E).

Intriguingly, we also observe *S100a4* expression specifically in the PDGFRA-positive dermal cells directly beneath eccrine placodes, which exhibit characteristic *En1* upregulation (Figure 3F, G). These *S100a4*-positive dermal cells are not morphologically distinct from the surrounding mesenchyme, consistent with previous reports that developing eccrine glands are never found in association with the dermal aggregates characteristic of the other major ectodermal appendages such as the hair follicle (Figure 3G)[8,10,21]. We find that the upregulation of *S100a4* in the eccrine placode-associated dermis is also dependent on epidermal *En1* since En1-cKO volar skin lacks dermal foci of *S100a4* including under the hair follicle placodes that populate the interfootpad space of this genotype (Figure 3G). By contrast, *S100a4* expression is retained in the ventral foot tendons of En1-cKO mice, indicating that its absence in the En1-cKO volar skin is specific to this context (Figure S4C). Lineage tracing of the *S100a4*-expressing dermal cells under the eccrine placode reveals that that the descendants of these cells not only give rise to the nascent gland-associated dermal cells captured in cluster 20, but also to descendants that surround the mature eccrine gland (Figure 3H, I). We therefore conclude that epidermal *En1* expression is required for the induction of a single, eccrine-associated, dermal lineage.

Eccrine-associated dermal lineage is conserved to humans

En1 expression in the limb ectoderm initiates well before the onset of eccrine gland formation in this tissue and persists in the adult, after development is completed[26,29,46] (Figure 4A, bottom). In contrast, we find that *S100a4* expression in the dermis proximal to the eccrine glands is restricted to the developmental period during which the epidermis is actively forming these appendages (Figure 4A, top). Accordingly, we find no evidence of *S100a4* expression either prior to eccrine placode formation or around the mature eccrine glands of adult mice (Figure 4A). This pattern is recapitulated in human skin, in which we observe *S100a4* expression in the dermal fibroblasts associated with eccrine placodes and nascent glands (120 gestational days, plantar foot skin; Figure 4B) but not in the dermal cells proximal to the mature gland (64 years old, cheek skin; Figure 4C). Thus, the eccrine-associated dermal lineage appears in conjunction with the activation of the *En1*-dependent epidermal eccrine developmental program in both mice and humans and undergoes progressive changes in gene expression over the course of eccrine gland formation. Collectively, these data implicate an evolutionarily conserved and transcriptionally distinct dermal lineage that is specifically associated with developing eccrine glands.

An *En1*-dependent eccrine niche (EDEN) is required for eccrine gland development

In light of finding that the *En1*-dependent dermal populations derive from a single lineage, and the specific association of these populations with developing eccrine glands in the

Author Manuscript Author Manuscript Author Manuscript Author Manuscript

epidermis, we interrogated the snRNA-seq data for evidence of signaling between the epidermal and dermal nuclei from Control samples. We first performed subclustering (Derm0-Derm11) and lineage pseudotime inference on all dermal nuclei to resolve putative developmental relationships within the broader dermal dataset (Figure 5A, B). We identify an inferred dermal lineage that terminates in subcluster Derm10, which corresponds to the validated, nascent gland-associated, dermal population represented in cluster 20 from the original analysis (Figure 3A, 5B). This lineage originates in Derm3, and successively progresses through Derm6, Derm9, and Derm2, before terminating in Derm10 (Figure 5B).

Having identified the subset of dermal nuclei that constitute the putative eccrine-associated dermal lineage, we performed cell-cell interaction modeling between this subset of dermal clusters and those which make up the validated eccrine epidermal lineage (Epi0, Epi3, Epi5, and Epi8; Figure 2G) using CellChat[47]. We detect 185 significant receptor-ligand pairs from 32 pathways among the eccrine-associated dermal and epidermal subclusters ($p < 0.05$; Figure 5C; Figure S5A, B; Data S2). Of these, we identify 52 significant receptor-ligand interactions from 14 pathways that employ secreted signaling factors, including the WNT, BMP, TGFBeta, and non-canonical WNT (ncWNT) pathways (Figure S5A,B; Data S2). We identify receptor-ligand pairings consistent with bidirectional crosstalk between the lineages, with the epidermal lineage signaling to the dermal lineage and vice versa (Figure 5C; Figure S5A, B). Moreover, we find that the signals mediating these interactions change over developmental time (Figure 5C; Figure S5A, B).

The signaling interactions predicted from the snRNA-seq expression data suggest that the dermal and epidermal eccrine lineages engage in reciprocal crosstalk over the course of eccrine development. This finding is intriguing given the well-established importance of dermal-ectodermal interactions for the developmental progression of other major ectodermal appendages, such as the hair follicle and mammary gland[8]. Accordingly, we tested whether the *En1*-dependent dermal population is required for eccrine gland formation. For this purpose, we made use of the specific expression of *S100a4* in the mouse volar dermis to mark this population (Figure 3C-G, 4A; Data S1C).

Using an inducible genetic system, we ablated *S100a4*-expressing cells at the onset of eccrine gland development using targeted expression of diphtheria toxin subunit alpha (DTA) and assessed eccrine gland density in the volar skin of Control (S100a4-CreERT2/+;DTA/+ or DTA/DTA) as compared to Ablated (S100a4-CreERT2/+;DTA/DTA or S100a4-CreERT2/S100a4-CreERT2;DTA/DTA) mice[48]. Timed pregnant females were dosed with tamoxifen to induce Cre activation at E14.5 and E15.5 to specifically ablate *S100a4* expressing cells around the time of footpad eccrine placode formation[9,11,12]. At E19.5, when footpad eccrine glands are at the nascent stage, we quantified eccrine gland density in the footpads of Control and Ablated mice (Figure 5D)[11]. This endpoint was selected due to dystocia in the dams, which necessitated end-point cesarean section to deliver pups for analysis.

We observe a deficit of *S100a4* positive cells in the footpads of Ablated genotypes as compared to Controls (Figure 5E). Notably, *En1* expression persists in both Control and Ablated groups (Figure 5E). The impact of depleting the *S100a4* expressing dermal cells on

Author Manuscript Author Manuscript Author Manuscript Author Manuscript

eccrine gland development is striking. We find that eccrine gland density is on average 45% lower in Ablated compared to Control animals (Wilcoxon-Mann-Whitney test: $p = 0.0284$, $Z = 2.1909$, $r = 0.66$; Control: $n = 5$, Ablated: $n = 6$) (Figure 5E,F). Importantly, eccrine glands still present in Ablated animals retained normal *S100a4* expression around the gland, indicating that the population was not effectively depleted in these regions (Figure S5C). Taken together, our findings identify an *En1*-dependent eccrine niche (EDEN) in the dermis, direct proximity to which is required for eccrine gland development in the epidermis to proceed (Figure 6A).

Discussion

In “The Variation of Animals and Plants Under Domestication”, Charles Darwin describes a family in Sindh (in present-day Pakistan) “in which ten men…were furnished, in the course of four generations…with only four small and weak incisor teeth and with eight posterior molars…have very little hair on the body, and … suffer much during hot weather from excessive dryness of the skin”[49]. One of the earliest formal accounts to suggest an underlying link between the formation of the group of organs we call ectodermal appendages, Darwin’s description also aptly captures the importance of eccrine glands in human physiology. More than 150 years later, our study uncovers a blueprint for eccrine gland development and identifies transcriptional and cellular transitions at which the ectodermal appendage developmental paradigm diverges to build these essential organs (Figure 6A).

Duality and temporal transitions in the eccrine gland epidermal program during development

We find that the upregulation of epidermal *En1* is necessary for a transcriptional signature that distinguishes the eccrine placode from that of the hair follicle. That this signature includes upregulation of the Wnt inhibitor *Dkk4* is intriguing since previous studies have postulated that differences in the levels of canonical Wnt signaling determine the fate of ectodermal appendage placodes, with hair placodes proposed to require the highest level of Wnt signaling among the different appendage types[12,43,50,51]. We find that the restricted upregulation of *Dkk4* to the eccrine placode is associated with the formation of more eccrine glands in mice (Figure 2K, L). This suggests that spatial as well as quantitative parameters are integrated into the transcriptomic signature of the eccrine placode. Consistent with this, placode-specific *Dkk4* expression is critical for the reaction diffusion mechanism regulating the formation of skin appendages and disruption of this pattern through ectopic expression of this gene throughout the basal epidermis was reported to reduce eccrine gland density[10,43]. Resolving the functional importance of patterned *Dkk4* upregulation and of the other *En1*-dependent transcriptional changes we identified will set the stage for uncovering the intrinsic program that confers eccrine identity in the epidermis.

The relative paucity of the specialized eccrine transcriptome as compared to the bulk of placodal transcripts that are shared between eccrine gland and hair follicle progenitors during early development contrasts with the expression profile of later stages. Our data indicate that as development proceeds, differentiation of the eccrine cell types is coupled

Author Manuscript Author Manuscript Author Manuscript Author Manuscript

with a concomitant shift in the balance of the eccrine transcriptome towards a more specialized and distinctive expression profile (Figure 6A).

The extensive overlap we find in the transcriptome of hair and eccrine placodes may help to explain why previous efforts have also identified a largely shared set of signals in the early development of ectodermal appendages, irrespective of type[8,10,12,14,52,53]. In particular, the relative dearth of eccrine placode-enriched transcripts as compared to the far greater pool of those that are generalized across hair and eccrine types has intriguing implications for the character of the elusive, first dermal signal that triggers appendage fate and formation[12,54-56]. Our observations raise the possibility that the first inductive signal from the dermis, which initiates eccrine development is also dualistic in nature. Given the relative proportions of the two classes of placodal transcripts captured in our study, the eccrine dermal signals may show a similar skew. This would in turn reduce the power to detect the specialized dermal inducers within the context of the greater proportion of those that are generalized across the different appendage types. The identification of the subset of transcripts that are differentially enriched in eccrine versus hair follicle placodes provides a directed means to parse out the precise composition of these upstream signals from the dermis.

EDEN – a dermal niche for eccrine development

We find that the progression of the epidermal program in the eccrine placode requires the presence of EDEN, a dermal niche for eccrine glands (Figure 6A). Importantly, our data suggest that EDEN is not the source of the first dermal inductive signal that initiates placode formation. That the transcriptional identity of EDEN depends on the upregulation of ectodermal *En1*, and that EDEN is found in association with eccrine gland epidermal anlagen, but not other *En1*-expressing cells, suggests that EDEN is analogous to the dermal condensations that form in response to the placodes of other major appendages such as teeth and hair follicles[8]. Future experiments to distinguish between the roles of *En1* in the placode as opposed to the inter-appendage epidermis in the induction of EDEN will help to clarify this. A starting point for these investigations and for functional dissection of the signals mediating interactions between the developing eccrine glands and the niche are the candidate factors identified in this study. It is also important to understand whether the EDEN lineage is required for eccrine development and homeostasis beyond the placode stage in order to establish its closest functional homology to the niches of other appendages. This is because while the hair follicle dermal condensate (and its derivative the dermal papilla) is persistently required, the dense mesenchyme that directs early mammary gland development is transient and its role supplanted by the fat pad during the later stages of mammogenesis[8,52].

Irrespective of the precise source in the epidermis, our data demonstrate that a cell-autonomous transcriptional repressor, EN1, which is expressed in the basal epidermis, is required to induce a distinct cellular identity in the underlying dermal compartment. There is precedence for this, as evidenced by the early and the separable role of ectodermal *En1* in maintaining the identity of the ventral limb bud by inhibiting mesenchymal *Lmx1b* expression[19,26,57]. In this context, *En1* acts by inhibiting *Wnt7a* in the ventral limb

Author Manuscript Author Manuscript Author Manuscript Author Manuscript

ectoderm[57]. Having identified a pool of *En1*-dependent transcripts in the eccrine placode and in the skin basal epidermis, our findings make it possible to determine whether *En1* effects are mediated by similar or entirely independent effectors in ectodermal appendage development. Future studies to interrogate the function of these EN1 targets are also important to understand and distinguish between EN1's roles in specifying the dermal niche, and in directly acting on the epidermal populations that make up the gland itself.

Intriguingly, we find that despite the continued expression of *En1* in adult basal keratinocytes in the eccrine forming regions and in the mature eccrine glands themselves, the expression of *S100a4*, which specifically marks the EDEN lineage throughout the eccrine developmental period, does not persist in its descendants around the mature eccrine glands of either mice or humans[29,58]. This suggests that the dermal niche, at least as it exists during development, may not be retained once eccrine gland formation is completed and may help to explain why eccrine glands exhibit limited ability to regenerate[9]. Previous studies have demonstrated the existence of several, unipotent stem cell populations within the mature eccrine gland, in the duct and the secretory coils, respectively[9]. In response to injury, these stem cells can only be mobilized to repair their respective lineages, but not the whole gland[9]. Comparing the functional properties of EDEN lineage cells and the significance of gene expression changes therein during eccrine gland development and homeostasis may help to resolve the contribution of extrinsic factors to this regenerative limitation.

Notably, the hair follicle dermal niche is not only necessary for the regeneration of the hair follicle but is also sufficient to induce epithelial cells to form *de novo* hair follicles, even in adulthood[59,60]. It is intriguing to speculate that EDEN may have comparable properties with respect to inducing *de novo* eccrine gland formation. Understanding whether the molecular effectors of EDEN demonstrate such eccrine-inducing capabilities has the potential to seed efforts to repair wounds and burns with skin regenerates that contain eccrine glands. Coupled with the capture of an eccrine epidermal transcriptome during development, the identification of EDEN not only addresses the long-standing developmental question of how the dermal and epidermal skin compartments of mammalian skin are differentially mobilized to build eccrine glands, but also sets the stage for meeting a critical need in human regenerative medicine.

Limitations of the study

Our study analyzes the nuclear transcriptome, which represents a fraction of the total transcriptome of the cell. Therefore, there may be additional differential transcripts that are not captured by our study. Despite this, the validations we performed indicate our findings from the nuclear transcriptome are biologically relevant and are representative of the heterogeneity in developing eccrine glands.

Author Manuscript Author Manuscript Author Manuscript Author Manuscript

STAR METHODS

Resource availability

Lead contact—Further information and requests for resources and reagents should be directed to and will be fulfilled by the corresponding author, Yana G. Kamberov (yana2@pennmedicine.upenn.edu).

Materials availability—This study did not generate new, unique reagents.

Data and code availability—Raw and processed snRNA-seq data files have been deposited in NCBI's the Gene Expression Omnibus[61] and are accessible through GEO Series accession number GSE220977 (https://www.ncbi.nlm.nih.gov/geo/query/acc.cgi?acc=GSE220977). Any additional information required to reanalyze the data reported in this paper is available from the lead contact upon request.

Experimental model and study participant details

Animals—*Tg(tetO-cre)1Jaw/J (tetO-Cre)*[32] and *Gt(ROSA)26Sor*$^{tm1(DTA)Lky}$*/J* (ROSA-DTA)[48] mice were purchased from the Jackson Laboratory. *Tg(KRT5-rtTA)T2D6Sgkd/J* (Krt5-rtTA)[33] mice were provided by Dr. Sarah Millar (Icahn School of Medicine at Mount Sinai), *En1tm8.1Alj/J* (En1^{flox})[31] mice were provided by Dr. Alexandra Joyner (Memorial Sloan Kettering Cancer Center) and *Lgr6tm2.1(cre/ERT2)Cle/J* (Lgr6-eGFP)[62] and *Gt(ROSA)26Sor*$^{tm14(CAG-tdTomato)Hze}$/J (ROSA-tdTomato)[63] mice were provided by Dr. Pantelis Rompolas (University of Pennsylvania). S100a4-CreERT2 mice were generated by Dr. Mayumi Ito (New York University) and provided under material transfer agreement. *Gt(ROSA)26Sortm4(ACTB-tdTomato,-EGFP)Luo/J* (mTmG)[64] mice were provided by Dr. George Cotsarelis (University of Pennsylvania). En1^{flox}, Krt5-rtTA, and tetO-Cre mice were maintained on an FVB/N background (Charles River Laboratories) for more than 10 generations. ROSA-DTA mice were maintained on a C57BL/6J background (Jackson Laboratory) until they were bred to S100a4-CreERT2 mice, which were maintained on a mixed genetic background. Lgr6-eGFP mice were also maintained on a mixed genetic background. FVB/N and C57BL/6N wild type mice were obtained from Charles River Laboratories and Taconic Biosciences, respectively. Both males and females were used for all experiments in this study.

For inducible En1 conditional knock-out (En1-cKO) experiments, male mice harboring the tetO-Cre, Krt5-rtTA, and homozygous En1^{flox} alleles were mated to females homozygous for En1^{flox} and carrying the Krt5-rtTA allele. Timed pregnant dams were continuously administered a doxycycline dosed diet (6 g/kg) *ad libidum* beginning at E16.5. Offspring were euthanized at either P2.5 or P28 via decapitation or CO_2 inhalation, respectively.

For embryonically induced S100a4 lineage tracing experiments, male S100a4-CreERT2/+ mice were mated to ROSA-tdTomato homozygous females. Timed pregnant females were dosed with tamoxifen in corn oil via oral gavage (3 mg/kg) at E15.5 and pups were euthanized at P2.5 for volar hindpaw collection. For perinatally induced S100a4 lineage tracing, male S100a4-CreERT2/+;mTmG/+ mice were mated to mTmG/+ or mTmG/mTmG females and pups were dosed orally with tamoxifen dissolved in corn oil (10μl of 50mg/ml

Author Manuscript Author Manuscript Author Manuscript Author Manuscript

stock) at P1.5 and P2.5, coinciding with placode stage of IFP eccrine glands in the volar skin, and volar skin from the forelimb and hindlimb was harvested at P22.

For S100a4+ cell ablation experiments, male mice harboring at least one copy of the S100a4-CreERT2 and ROSA-DTA alleles were mated to females either homozygous for ROSA-DTA or heterozygous for both S100a4-CreERT2 and ROSA-DTA. Timed pregnant females were dosed with tamoxifen in corn oil via oral gavage (3 mg/kg) at both E14.5 and E15.5. Pregnant dams were euthanized at E19.5 (developmental equivalent of P0) and pups were harvested via endpoint caesarean section due to dystocia in the dams.

All mice used in this study were housed on a 12h light/dark cycle in a University Laboratory Animal Resources (ULAR) managed vivarium at the Perelman School of Medicine (PSOM). All procedures were performed in accordance with guidelines established by the National Institutes of Health and have been approved by the University of Pennsylvania PSOM Institutional Animal Care and Use Committee (protocol # 806105). Mice were housed under standard laboratory conditions and received food and water *ad libitum*.

Human tissue—Specimens from fetal (120 gestational days) human plantar foot skin were obtained from the Birth Defects Research Laboratory at the University of Washington (Uniform Biological Material Transfer Agreement #48286A) with ethics board approval and maternal written consent. Deidentified samples from adult human cheek skin (64 years old) were obtained from the Skin Biology and Disease Resource Center at the University of Pennsylvania with ethics board approval and written consent. This study was performed in accordance with ethical and legal guidelines of the University of Pennsylvania institutional review board.

Method details

Quantification of appendages in adult volar skin—Quantification of eccrine glands and hair follicles at P28 was performed in whole mount preparations of hindlimb volar skin as previously described[16]. Briefly, the epidermis was separated from the underlying dermis by dispase digestion and fixed with 10% neutral buffered formalin. Hair follicle-associated sebaceous glands were stained with Oil Red O and appendages (eccrine glands and hair follicles) were stained with Nile Blue, and whole mounts were imaged on a Leica M680 dissection scope fitted with a Leica IC90E camera. All data reported in this manuscript represents the average counts from the right and left hindlimb volar skin of an individual mouse.

Isolation and purification of nuclei for snRNA-seq—En1-cKO and Control pups were euthanized at P2.5 and volar hindlimb skin (right and left) was rapidly dissected on ice and snap frozen on dry ice and stored at −80°C until nuclear isolation. Single nuclear suspensions were generated from the pooled volar hindlimb skin (right and left) from 5 mice of the same genotype, for a total of 10 pooled volar skins, as previously described with some modifications[35]. Pooled samples were dissociated in homogenization buffer using a Polytron homogenizer (Kinematica Inc.) followed by dounce homogenization (20 times with loose pestle; 10 times with tight pestle). Suspensions were filtered to remove debris and single nuclear suspensions were quantified via hemocytometer after staining with Trypan

Author Manuscript Author Manuscript Author Manuscript Author Manuscript

Blue, which stains all nuclei. For P2.5 volar skin, we obtained ≥ $2.1x10^5$ nuclei/ml for each sample. Sucrose gradient centrifugation was not performed on single nuclear suspensions. Biological replicates were prepared and sequenced in two separate batches; one replicate of each genotype (En1-cKO: tetO-Cre/+; Krt5-rtTA/+; $En1^{flox/flox}$; Control: $En1^{flox/flox}$, Krt5-rtTA/+; $En1^{flox/flox}$) was processed and sequenced in the same batch to avoid autocorrelation of condition and batch effects.

snRNA-seq library preparation and sequencing—Single nuclei were co-encapsulated with barcoded beads (ChemGenes) and reverse transcription was performed as previously described[35]. Optimal PCR cycle number for library amplification was determined via qPCR using 6,000 beads, cDNA was tagmented, and libraries were further amplified as previously described[35]. cDNA libraries were quantified via Qubit 3.0 (Invitrogen) and library quality was determined via Bioanalyzer (Agilent) prior to sequencing on an Illumina NextSeq 500 using the 75-cycle High Output v2 kit (Illumina). In total, six neonatal volar skin snRNA-seq libraries were sequenced in four sequencing runs. See open access snRNA-seq protocol for more details: https://www.protocols.io/view/snucdrop-seq-protocol-n2bvjr36plk5/v2[35].

***In situ* hybridization, immunofluorescence, RNAscope, and imaging—**Volar skin was fixed in 4% PFA, cryoprotected using sucrose, and embedded in OCT (Tissue Tek) for cryo-sectioning at a thickness of 10-12 μm. Sections were collected in 3-4 series for staining of adjacent sections. *In situ* hybridization was performed as previously described[19] with custom anti-sense DIG-labeled riboprobes transcribed *in vitro* (Roche) from amplified cDNA (see Key Resources Table for primers). Immunofluorescence was performed for KRT14 (1:10,000, BioLegend 905303), EDAR (1:100, R&D Systems AF745), PDGFRA (1:100, R&D Systems AF1062), and GFP (1:1000, Abcam ab13970) after blocking tissue in PBT (0.2% Triton-X100 in PBS) with 10% serum. Secondary detection was performed with antibodies conjugated to Alexa $Fluor^{488}$ (Invitrogen A-11039 or Abcam ab150129), Alexa $Fluor^{594}$ (Jackson ImmunoResearch 711-585-152), or Alexa $Fluor^{647}$ (Jackson ImmunoResearch 711-605-152) and samples were counterstained with 4′6-diamidino-2-phenylindole (DAPI, Sigma D9542).

FFPE adult and fetal human tissue was processed and sectioned by SBDRC Core A. RNAscope was performed on 5 μm paraffin sections after standard target retrieval for *S100A4* (ACD Bio #422071), *PPIB* (positive control; ACD Bio #313901), and *DapB* (negative control; ACD Bio #310043) using an RNAscope 2.5 HD-RED assay kit (ACD Bio #322350). Subsequently, immunofluorescence for KRT14 was performed as described above and samples were counterstained with DAPI.

Samples were imaged on a Leica DM5500B microscope equipped with Leica DFC 500 (bright field) and Leica DFC 360X (fluorescence) cameras. Images were processed using FIJI software[65].

Scoring of footpad eccrine glands at E19.5—*S100a4* Ablated and Control samples were harvested as described above and whole hindlimbs were cryo-sectioned at 10 μm and three adjacent series of sections were collected. The first series was stained with

Author Manuscript Author Manuscript Author Manuscript Author Manuscript

hematoxylin and eosin (H&E, Sigma Aldrich) for scoring. The second and third series were used for *in situ* hybridization for *En1* and *S100a4*, respectively, to confirm efficient ablation of *S100a4*+ cells. Scoring of E19.5 Hematoxylin and eosin-stained sections was performed by counting all nascent eccrine glands in the footpads throughout the entire series of sections. Eccrine counts were then normalized to the number of sections scored to yield an eccrine density estimate.

RNA extraction and qRT-PCR—FVB/N and C57BL6/N neonatal pups were euthanized at P2.5 and volar hindpaw skin was harvested and snap frozen as described above. Biological replicates are comprised of left and right hindpaw skin pooled from 3 mice. Pooled skin samples were dissociated using a Polytron homogenizer and total RNA was isolated using TRIzol (Life Technologies) extraction followed by clean up and on-column DNase I treatment using a RNeasy Mini Kit (Qiagen). cDNA was reverse transcribed using SuperScript III (Thermo Fisher) following the manufacturer's instructions. qRT-PCR was performed in biological triplicate and technical quadruplicate using Power SYBR PCR master mix (Thermo Fisher) for *Dkk4* and *En1. Rpl13a* served as a reference gene for normalizing Ct values. Each data point reported in Figure 2L represents the mean of technical replicates for a sample. Primers used for qRT-PCR are found in Table S4.

Quantification and statistical analysis

snRNA-seq data pre-processing—Paired-end snRNA-seq reads were processed using publicly available the Drop-seq Tools v1.12 software[66] with modifications described previously[35]. A digital expression matrix was generated by assembling a list of UMIs in each gene (as rows) within each cell (as columns), and UMIs within ED = 1 were merged.

snRNA-seq cluster identification and marker gene analysis—Digital expression matrices for each sample were loaded into Seurat v4.0.2[67] and merged. UMI counts were normalized by scaling by library size, multiplying by 10,000, and transforming to log scale. Genes were filtered out if they were expressed in <10 nuclei and nuclei were filtered out if they contained a high proportion of UMIs mapped to mitochondrial genes (≥0.05), fewer than 300 or more than 6000 detected genes, resulting in 45,370 nuclei in the final filtered dataset.

Prior to clustering, individual sample datasets were integrated using the Harmony algorithm[37], the top 2000 variable genes were identified using the *FindVariableFeatures* function in Seurat with the VST selection method, and expression of these variable genes was scaled and centered for principal components analysis. Based on the cumulative standard deviations of each principal component (PC), visualized by the function *ElbowPlot* in Seurat, we selected the first 40 PCs for two-dimensional uniform manifold approximation and projection (UMAP) implemented by Seurat *RunUMAP* with default parameters. Initial clustering on the full dataset (all nuclei, merged conditions) identified 23 clusters with the resolution parameter for *FindClusters* set to 0.7. Based on the expression pattern of well-established marker genes in this dataset, we assigned 25,859 nuclei to dermal cells (~57% of our data), 9,070 nuclei to epidermal cells (~20% of our data), and 10,441 nuclei to various other cell types (see Figure S2). Differential expression analysis was performed

Author Manuscript Author Manuscript Author Manuscript Author Manuscript

to identify marker genes for each of these 23 initial clusters using Seurat's *FindAllMarkers* function with Wilcoxon test. Differentially upregulated genes that were expressed in at least 25% of nuclei with a log fold change (LFC) ≥ 0.58 were considered marker genes (Data S1A). Dermal cluster specific marker genes were identified using the same approach, but with only dermal clusters of nuclei compared to each other (Data S1C).

Subclustering, pseudobulk differential expression, trajectory inference, and CellChat analysis—Nuclei from clusters determined to be epidermal (original clusters 2, 9,10,14, and 15) or dermal (original clusters 0, 1, 3, 4, 5, 8, 11, 20) were subsetted, the top 2000 variable genes were identified, and PCA was performed as above. The top 40 PCs were selected for clustering analysis with a resolution of 0.4 for epidermal nuclei and 0.7 for dermal nuclei, leading to the identification of 9 epidermal subclusters and 11 dermal subclusters. Of these 9 epidermal subclusters, 6 are basal (6,799 nuclei) and 3 of these subclusters are suprabasal (2,271 nuclei). Marker genes of each subcluster were identified as described above (Data S1B, C) and gene ontology (GO) enrichment analysis was performed on these marker gene lists using the *compareCluster* function from the Cluster Profiler R package[68].

We performed pseudo-bulk analysis to identify differentially expressed transcripts between Control and En1-cKO placode nuclei (Epi3). Pseudobulk samples were created using the Seurat function *PseudobulkExpression* on sample counts for each subcluster using the aggregate pseudo-bulk method. Differential expression analysis was performed on these pseudo-bulk samples for Epi3 using DESeq2[69] with a likelihood ratio test. Genes were deemed significantly differentially expressed between Control and En1-cKO pseudo-bulk samples if p adjusted < 0.01 and LFC ≥ 0.58.

Trajectory inference of the subclustered nuclei was performed using Slingshot[70] on either the subsetted epidermal or dermal PCA reduction (merged conditions). Epi0 was supplied as the starting cluster to the *slingshot* function for the epidermal trajectory inference; for dermal trajectory inference, subcluster Derm11 was provided as the end cluster. The inferred lineages were then mapped onto UMAP embeddings for visualization using the *embedCurves* Slingshot function. Differential progression analysis was performed on the epidermal lineage via Kolmogorov-Smirnov test of the lineage pseudotime distributions between Control and En1-cKO nuclei.

CellChat[47] was performed on Control nuclei from the dermal and epidermal subclusters that were determined to be involved in the relevant inferred lineages using the default CellChat mouse database. Average gene expression per cluster was computed using the "truncatedMean" method (trim=0.1) within CellChat's *computeCommunProb* function. All significant receptor-ligand interactions ($p < 0.05$) identified between any pair of clusters are summarized as a chord diagram (Figure 4C). Complete results are provided as a supplemental data file (Data S2).

Statistical analysis of phenotypic data and qRT-PCR expression—Statistical parameters, including sample sizes, are reported in figures, figure legends, tables, and/or corresponding results text. A Kruskal-Wallis test followed by a *post-hoc* Dunn's test with

Author Manuscript Author Manuscript Author Manuscript Author Manuscript

Benjamini-Hochberg correction for multiple comparisons was performed on P28 appendage counts for En1-cKO phenotyping (alpha = 0.05). A Mann-Whitney-Wilcoxon test was used for pairwise comparisons of qRT-PCR data (alpha = 0.05). All statistical analyses were performed in R[71].

Supplementary Material

Refer to Web version on PubMed Central for supplementary material.

ACKNOWLEDGMENTS

The authors thank Eric F. Joyce, Cliff Tabin, Pantelis Rompolas, Gabriella Rice, Sixia Huang, Paola Kuri, Stephanie Tsai, Elizabeth Grice, George Cotsarelis, Ed Morrissey, and Sarah Tishkoff for helpful discussions on this study. The authors thank Cliff Tabin, Marisa S. Bartolomei, Matthew Weitzman, Arjun Raj, and Klaus H. Kaestner for critical feedback on the manuscript. The authors thank Stacie Bumgarner for assistance with scientific illustration. We thank the Penn Skin Biology and Disease Resource Center (SBDRC) for use of Core A (P30-AR069589). HLD was supported by a National Institutes of Arthritis Musculoskeletal and Skin Diseases of the NIH (NIAMS) 5T32AR007465 award. SMM was supported by the Penn Academy for Skin Health and the SBDRC (P30-AR069589). HW was supported by a National Human Genome Research Institute of the NIH U01-HG012047 award. IAG was supported by a National Institute for Childhood Health and Disease of the NIH Award R24HD000836. YGK was supported by a SBDRC Pilot and Feasibility Award (P30-AR069589), a National Science Foundation (NSF) BCS-1847598 award, and a National Institute of Arthritis Musculoskeletal and Skin Diseases of the NIH Award R01AR077690. Any opinions, findings, and conclusions or recommendations expressed in this material are those of the authors and do not necessarily reflect the views of the NSF. The content is solely the responsibility of the authors and does not necessarily represent the official views of the NIH.

REFERENCES

1. Kuno Y. (1956). Human perspiration (Thomas).
2. Montagna William and Parakhal Paul F. (1974). The Structure and Function of Skin - 3rd Edition (Elsevier Inc.).
3. Kamberov YG, Guhan SM, DeMarchis A, Jiang J, Wright SS, Morgan BA, Sabeti PC, Tabin CJ, and Lieberman DE (2018). Comparative evidence for the independent evolution of hair and sweat gland traits in primates. Journal of Human Evolution 125, 99–105. 10.1016/j.jhevol.2018.10.008. [PubMed: 30502901]
4. Lu C, and Fuchs E (2014). Sweat Gland Progenitors in Development, Homeostasis, and Wound Repair. Cold Spring Harbor Perspectives in Medicine 4, a015222–a015222. 10.1101/cshperspect.a015222. [PubMed: 24492848]
5. Cui C-Y, and Schlessinger D (2015). Eccrine sweat gland development and sweat secretion. Experimental dermatology 24, 644. 10.1111/exd.12773. [PubMed: 26014472]
6. Montagna W, Ellis RA, and Silver A (1962). Advances in Biology of Skin Vol. III, Eccrine Sweat Glands and Eccrine Sweating (Pergamon Press Inc.).
7. Bayuo J. (2017). Management strategies of burns associated hyperthermia: A case report. Burns Open 1, 45–47. 10.1016/j.burnso.2017.05.011.
8. Biggs LC, and Mikkola ML (2014). Early inductive events in ectodermal appendage morphogenesis. Seminars in Cell & Developmental Biology 25–26, 11–21. 10.1016/j.semcdb.2014.01.007.
9. Lu CP, Polak L, Rocha AS, Pasolli HA, Chen S-C, Sharma N, Blanpain C, and Fuchs E (2012). Identification of Stem Cell Populations in Sweat Glands and Ducts: Roles in Homeostasis and Wound Repair. Cell 150, 136–150. 10.1016/j.cell.2012.04.045. [PubMed: 22770217]
10. Cui C-Y, Yin M, Sima J, Childress V, Michel M, Piao Y, and Schlessinger D (2014). Involvement of Wnt, Eda and Shh at defined stages of sweat gland development. Development 141, 3752–3760. 10.1242/dev.109231. [PubMed: 25249463]
11. Taylor DK, Bubier JA, Silva KA, and Sundberg JP (2012). Development, Structure, and Keratin Expression in C57BL/6J Mouse Eccrine Glands. Vet Pathol 49, 146–154. 10.1177/0300985811430511. [PubMed: 22135020]

Author Manuscript Author Manuscript Author Manuscript Author Manuscript

12. Lu CP, Polak L, Keyes BE, and Fuchs E (2016). Spatiotemporal antagonism in mesenchymal-epithelial signaling in sweat versus hair fate decision. Science 354, aah6102. 10.1126/science.aah6102. [PubMed: 28008008]
13. Plikus M, Wang WP, Liu J, Wang X, Jiang T-X, and Chuong C-M (2004). Morpho-Regulation of Ectodermal Organs. The American Journal of Pathology 164, 1099–1114. 10.1016/S0002-9440(10)63197-5. [PubMed: 14982863]
14. Andl T, Reddy ST, Gaddapara T, and Millar SE (2002). WNT signals are required for the initiation of hair follicle development. Dev. Cell 2, 643–653. [PubMed: 12015971]
15. Mayer JA, Foley J, De La Cruz D, Chuong C-M, and Widelitz R (2008). Conversion of the Nipple to Hair-Bearing Epithelia by Lowering Bone Morphogenetic Protein Pathway Activity at the Dermal-Epidermal Interface. The American Journal of Pathology 173, 1339–1348. 10.2353/ajpath.2008.070920. [PubMed: 18832580]
16. Kamberov YG, Wang S, Tan J, Gerbault P, Wark A, Tan L, Yang Y, Li S, Tang K, Chen H, et al. (2013). Modeling Recent Human Evolution in Mice by Expression of a Selected EDAR Variant. Cell 152, 691–702. 10.1016/j.cell.2013.01.016. [PubMed: 23415220]
17. Headon DJ, and Overbeek PA (1999). Involvement of a novel Tnf receptor homologue in hair follicle induction. Nat. Genet 22, 370–374. 10.1038/11943. [PubMed: 10431242]
18. Headon DJ, Emmal SA, Ferguson BM, Tucker AS, Justice MJ, Sharpe PT, Zonana J, and Overbeek PA (2001). Gene defect in ectodermal dysplasia implicates a death domain adapter in development. Nature 414, 913–916. 10.1038/414913a. [PubMed: 11780064]
19. Kamberov YG, Karlsson EK, Kamberova GL, Lieberman DE, Sabeti PC, Morgan BA, and Tabin CJ (2015). A genetic basis of variation in eccrine sweat gland and hair follicle density. Proc. Natl. Acad. Sci. U.S.A 112, 9932–9937. 10.1073/pnas.1511680112. [PubMed: 26195765]
20. Aldea D, Kokalari B, Luckhart C, Aharoni A, Albert PR, and Kamberov YG (2019). The Transcription Factor Deaf1 Modulates Engrailed-1 Expression to Regulate Skin Appendage Fate. J Invest Dermatol 139, 2378–2381.e4. 10.1016/j.jid.2019.05.007. [PubMed: 31145909]
21. Widelitz RB, and Chuong C-M (1999). Early Events in Skin Appendage Formation: Induction of Epithelial Placodes and Condensation of Dermal Mesenchyme. Journal of Investigative Dermatology Symposium Proceedings 4, 302–306. 10.1038/sj.jidsp.5640234. [PubMed: 10674386]
22. Huh S-H, Närhi K, Lindfors PH, Häärä O, Yang L, Ornitz DM, and Mikkola ML (2013). Fgf20 governs formation of primary and secondary dermal condensations in developing hair follicles. Genes Dev. 27, 450–458. 10.1101/gad.198945.112. [PubMed: 23431057]
23. Biggs LC, Mäkelä OJ, Myllymäki S-M, Das Roy R, Närhi K, Pispa J, Mustonen T, and Mikkola ML (2018). Hair follicle dermal condensation forms via Fgf20 primed cell cycle exit, cell motility, and aggregation. eLife 7, e36468. 10.7554/eLife.36468. [PubMed: 30063206]
24. Mok K-W, Saxena N, Heitman N, Grisanti L, Srivastava D, Muraro MJ, Jacob T, Sennett R, Wang Z, Su Y, et al. (2019). Dermal Condensate Niche Fate Specification Occurs Prior to Formation and Is Placode Progenitor Dependent. Dev. Cell 48, 32–48.e5. 10.1016/j.devcel.2018.11.034. [PubMed: 30595537]
25. Gupta K, Levinsohn J, Linderman G, Chen D, Sun TY, Dong D, Taketo MM, Bosenberg M, Kluger Y, Choate K, et al. (2019). Single-Cell Analysis Reveals a Hair Follicle Dermal Niche Molecular Differentiation Trajectory that Begins Prior to Morphogenesis. Dev. Cell 48, 17–31.e6. 10.1016/j.devcel.2018.11.032. [PubMed: 30595533]
26. Loomis CA, Harris E, Michaud J, Wurst W, Hanks M, and Joyner AL (1996). The mouse Engrailed-1 gene and ventral limb patterning. Nature 382, 360–363. 10.1038/382360a0. [PubMed: 8684466]
27. Aldea D, Kokalari B, Atsuta Y, Dingwall HL, Zheng Y, Nace A, Cotsarelis G, and Kamberov YG (2023). Differential modularity of the mammalian Engrailed 1 enhancer network directs sweat gland development. PLOS Genetics 19, e1010614. 10.1371/journal.pgen.1010614. [PubMed: 36745673]
28. Aldea D, Atsuta Y, Kokalari B, Schaffner SF, Prasasya RD, Aharoni A, Dingwall HL, Warder B, and Kamberov YG (2021). Repeated mutation of a developmental enhancer contributed to human thermoregulatory evolution. PNAS 118. 10.1073/pnas.2021722118.

Author Manuscript Author Manuscript Author Manuscript Author Manuscript

29. Mainguy G, Ernø H, Montesinos ML, Lesaffre B, Wurst W, Volovitch M, and Prochiantz A (1999). Regulation of Epidermal Bullous Pemphigoid Antigen 1 (BPAG1) Synthesis by Homeoprotein Transcription Factors. Journal of Investigative Dermatology 113, 643–650. 10.1046/j.1523-1747.1999.00703.x. [PubMed: 10504454]

30. Glover JD, Sudderick ZR, Shih BB-J, Batho-Samblas C, Charlton L, Krause AL, Anderson C, Riddell J, Balic A, Li J, et al. (2023). The developmental basis of fingerprint pattern formation and variation. Cell 0. 10.1016/j.cell.2023.01.015.

31. Sgaier SK, Lao Z, Villanueva MP, Berenshteyn F, Stephen D, Turnbull RK, and Joyner AL (2007). Genetic subdivision of the tectum and cerebellum into functionally related regions based on differential sensitivity to engrailed proteins. Development 134, 2325–2335. 10.1242/dev.000620. [PubMed: 17537797]

32. Perl A-KT, Wert SE, Nagy A, Lobe CG, and Whitsett JA (2002). Early restriction of peripheral and proximal cell lineages during formation of the lung. Proc. Natl. Acad. Sci. U.S.A 99, 10482–10487. 10.1073/pnas.152238499. [PubMed: 12145322]

33. Diamond I, Owolabi T, Marco M, Lam C, and Glick A (2000). Conditional gene expression in the epidermis of transgenic mice using the tetracycline-regulated transactivators tTA and rTA linked to the keratin 5 promoter. J. Invest. Dermatol 115, 788–794. 10.1046/j.1523-1747.2000.00144.x. [PubMed: 11069615]

34. Habib N, Avraham-Davidi I, Basu A, Burks T, Shekhar K, Hofree M, Choudhury SR, Aguet F, Gelfand E, Ardlie K, et al. (2017). Massively parallel single-nucleus RNA-seq with DroNc-seq. Nat. Methods 14, 955–958. 10.1038/nmeth.4407. [PubMed: 28846088]

35. Hu P, Fabyanic E, Kwon DY, Tang S, Zhou Z, and Wu H (2017). Dissecting Cell-Type Composition and Activity-Dependent Transcriptional State in Mammalian Brains by Massively Parallel Single-Nucleus RNA-Seq. Molecular Cell 68, 1006–1015.e7. 10.1016/j.molcel.2017.11.017. [PubMed: 29220646]

36. Grindberg RV, Yee-Greenbaum JL, McConnell MJ, Novotny M, O'Shaughnessy AL, Lambert GM, Araúzo-Bravo MJ, Lee J, Fishman M, Robbins GE, et al. (2013). RNA-sequencing from single nuclei. Proceedings of the National Academy of Sciences 110, 19802–19807. 10.1073/pnas.1319700110.

37. Korsunsky I, Millard N, Fan J, Slowikowski K, Zhang F, Wei K, Baglaenko Y, Brenner M, Loh P, and Raychaudhuri S (2019). Fast, sensitive and accurate integration of single-cell data with Harmony. Nat Methods 16, 1289–1296. 10.1038/s41592-019-0619-0. [PubMed: 31740819]

38. Hirai Y, Nose A, Kobayashi S, and Takeichi M (1989). Expression and role of E- and P-cadherin adhesion molecules in embryonic histogenesis. I. Lung epithelial morphogenesis. Development 105, 263–270. 10.1242/dev.105.2.263. [PubMed: 2806125]

39. Mills AA, Zheng B, Wang X-J, Vogel H, Roop DR, and Bradley A (1999). p63 is a p53 homologue required for limb and epidermal morphogenesis. Nature 398, 708–713. 10.1038/19531. [PubMed: 10227293]

40. Pellegrini G, Dellambra E, Golisano O, Martinelli E, Fantozzi I, Bondanza S, Ponzin D, McKeon F, and De Luca M (2001). p63 identifies keratinocyte stem cells. Proceedings of the National Academy of Sciences 98, 3156–3161. 10.1073/pnas.061032098.

41. Driskell RR, Lichtenberger BM, Hoste E, Kretzschmar K, Simons BD, Charalambous M, Ferron SR, Herault Y, Pavlovic G, Ferguson-Smith AC, et al. (2013). Distinct fibroblast lineages determine dermal architecture in skin development and repair. Nature 504, 277–281. 10.1038/nature12783. [PubMed: 24336287]

42. Bazzi H, Fantauzzo KA, Richardson GD, Jahoda CAB, and Christiano AM (2007). The Wnt inhibitor, Dickkopf 4, is induced by canonical Wnt signaling during ectodermal appendage morphogenesis. Developmental Biology 305, 498–507. 10.1016/j.ydbio.2007.02.035. [PubMed: 17397822]

43. Sick S, Reinker S, Timmer J, and Schlake T (2006). WNT and DKK Determine Hair Follicle Spacing Through a Reaction-Diffusion Mechanism. Science 314, 1447–1450. 10.1126/science.1130088. [PubMed: 17082421]

44. Fliniaux I, Mikkola ML, Lefebvre S, and Thesleff I (2008). Identification of dkk4 as a target of Eda-A1/Edar pathway reveals an unexpected role of ectodysplasin as inhibitor of Wnt signalling in

Author Manuscript Author Manuscript Author Manuscript Author Manuscript

ectodermal placodes. Developmental Biology 320, 60–71. 10.1016/j.ydbio.2008.04.023. [PubMed: 18508042]

45. Zhang Y, Tomann P, Andl T, Gallant NM, Huelsken J, Jerchow B, Birchmeier W, Paus R, Piccolo S, Mikkola ML, et al. (2009). Reciprocal requirements for EDA/EDAR/NF-kappaB and Wnt/beta-catenin signaling pathways in hair follicle induction. Dev. Cell 17, 49–61. 10.1016/j.devcel.2009.05.011. [PubMed: 19619491]
46. Joyner AL, and Martin GR (1987). En-1 and En-2, two mouse genes with sequence homology to the Drosophila engrailed gene: expression during embryogenesis. Genes Dev. 1, 29–38. 10.1101/gad.1.1.29. [PubMed: 2892757]
47. Jin S, Guerrero-Juarez CF, Zhang L, Chang I, Ramos R, Kuan C-H, Myung P, Plikus MV, and Nie Q (2021). Inference and analysis of cell-cell communication using CellChat. Nat Commun 12, 1088. 10.1038/s41467-021-21246-9. [PubMed: 33597522]
48. Voehringer D, Liang H-E, and Locksley RM (2008). Homeostasis and Effector Function of Lymphopenia-Induced "Memory-Like" T Cells in Constitutively T Cell-Depleted Mice1 The Journal of Immunology 180, 4742–4753. 10.4049/jimmunol.180.7.4742. [PubMed: 18354198]
49. Darwin C. (1875). The variation of animals and plants under domestication. Second. (John Murray, Albemarle Street).
50. Dhouailly D. (2009). A new scenario for the evolutionary origin of hair, feather, and avian scales. J Anat 214, 587–606. 10.1111/j.1469-7580.2008.01041.x. [PubMed: 19422430]
51. Zhang Y, Andl T, Yang SH, Teta M, Liu F, Seykora JT, Tobias JW, Piccolo S, Schmidt-Ullrich R, Nagy A, et al. (2008). Activation of beta-catenin signaling programs embryonic epidermis to hair follicle fate. Development 135, 2161–2172. 10.1242/dev.017459. [PubMed: 18480165]
52. Mikkola ML, and Millar SE (2006). The mammary bud as a skin appendage: unique and shared aspects of development. J Mammary Gland Biol Neoplasia 11, 187–203. 10.1007/s10911-006-9029-x. [PubMed: 17111222]
53. Chu EY, Hens J, Andl T, Kairo A, Yamaguchi TP, Brisken C, Glick A, Wysolmerski JJ, and Millar SE (2004). Canonical WNT signaling promotes mammary placode development and is essential for initiation of mammary gland morphogenesis. Development 131, 4819–4829. 10.1242/dev.01347. [PubMed: 15342465]
54. Dhouailly D. (1973). Dermo-epidermal interactions between birds and mammals: differentiation of cutaneous appendages. Development 30, 587–603.
55. Dhouailly D. (1977). Regional specification of cutaneous appendages in mammals. Wilhelm Roux' Archiv 181, 3–10. 10.1007/BF00857264.
56. Ferraris C, Chevalier G, Favier B, Jahoda CA, and Dhouailly D (2000). Adult corneal epithelium basal cells possess the capacity to activate epidermal, pilosebaceous and sweat gland genetic programs in response to embryonic dermal stimuli. Development 127, 5487–5495. [PubMed: 11076768]
57. Cygan JA, Johnson RL, and McMahon AP (1997). Novel regulatory interactions revealed by studies of murine limb pattern in Wnt-7a and En-1 mutants. Development 124, 5021–5032. [PubMed: 9362463]
58. GTEx Consortium (2015). Human genomics. The Genotype-Tissue Expression (GTEx) pilot analysis: multitissue gene regulation in humans. Science 348, 648–660. 10.1126/science.1262110. [PubMed: 25954001]
59. Jahoda CA, Horne KA, and Oliver RF (1984). Induction of hair growth by implantation of cultured dermal papilla cells. Nature 311, 560–562. 10.1038/311560a0. [PubMed: 6482967]
60. Reynolds AJ, and Jahoda CA (1992). Cultured dermal papilla cells induce follicle formation and hair growth by transdifferentiation of an adult epidermis. Development 115, 587–593. [PubMed: 1425341]
61. Edgar R. (2002). Gene Expression Omnibus: NCBI gene expression and hybridization array data repository. Nucleic Acids Research 30, 207–210. 10.1093/nar/30.1.207. [PubMed: 11752295]
62. Snippert HJ, Haegebarth A, Kasper M, Jaks V, van Es JH, Barker N, van de Wetering M, van den Born M, Begthel H, Vries RG, et al. (2010). *Lgr6* Marks Stem Cells in the Hair Follicle That Generate All Cell Lineages of the Skin. Science 327, 1385–1389. 10.1126/science.1184733. [PubMed: 20223988]

Author Manuscript Author Manuscript Author Manuscript Author Manuscript

63. Madisen L, Zwingman TA, Sunkin SM, Oh SW, Zariwala HA, Gu H, Ng LL, Palmiter RD, Hawrylycz MJ, Jones AR, et al. (2010). A robust and high-throughput Cre reporting and characterization system for the whole mouse brain. Nat Neurosci 13, 133–140. 10.1038/nn.2467. [PubMed: 20023653]

64. Muzumdar MD, Tasic B, Miyamichi K, Li L, and Luo L (2007). A global double-fluorescent Cre reporter mouse. Genesis 45, 593–605. 10.1002/dvg.20335. [PubMed: 17868096]

65. Schindelin J, Arganda-Carreras I, Frise E, Kaynig V, Longair M, Pietzsch T, Preibisch S, Rueden C, Saalfeld S, Schmid B, et al. (2012). Fiji: an open-source platform for biological-image analysis. Nat Methods 9, 676–682. 10.1038/nmeth.2019. [PubMed: 22743772]

66. Macosko EZ, Basu A, Satija R, and others (2015). Highly parallel genome-wide expression profiling of individual cells using nanoliter droplets. Cell 161, 1202–1214. [PubMed: 26000488]

67. Hao Y, Hao S, Andersen-Nissen E, Mauck WM, Zheng S, Butler A, Lee MJ, Wilk AJ, Darby C, Zager M, et al. (2021). Integrated analysis of multimodal single-cell data. Cell 184, 3573–3587.e29. 10.1016/j.cell.2021.04.048. [PubMed: 34062119]

68. Wu T, Hu E, Xu S, Chen M, Guo P, Dai Z, Feng T, Zhou L, Tang W, Zhan L, et al. (2021). clusterProfiler 4.0: A universal enrichment tool for interpreting omics data. Innovation (Camb) 2, 100141. 10.1016/j.xinn.2021.100141. [PubMed: 34557778]

69. Love MI, Huber W, and Anders S (2014). Moderated estimation of fold change and dispersion for RNA-seq data with DESeq2. Genome Biol 15, 550. 10.1186/s13059-014-0550-8. [PubMed: 25516281]

70. Street K, Risso D, Fletcher RB, Das D, Ngai J, Yosef N, Purdom E, and Dudoit S (2018). Slingshot: cell lineage and pseudotime inference for single-cell transcriptomics. BMC Genomics 19, 477. 10.1186/s12864-018-4772-0. [PubMed: 29914354]

71. R Core Team (2022). R: A Language and Environment for Statistical Computing (R Foundation for Statistical Computing).

Author Manuscript Author Manuscript Author Manuscript Author Manuscript

Highlights

- Eccrine gland development requires EDEN, an evolutionarily conserved dermal niche.
- Eccrine and hair placode transcriptomes are predominantly congruent.
- An *En1*-dependent, low-abundance signature differentiates early eccrine identity.

Author Manuscript Author Manuscript Author Manuscript Author Manuscript

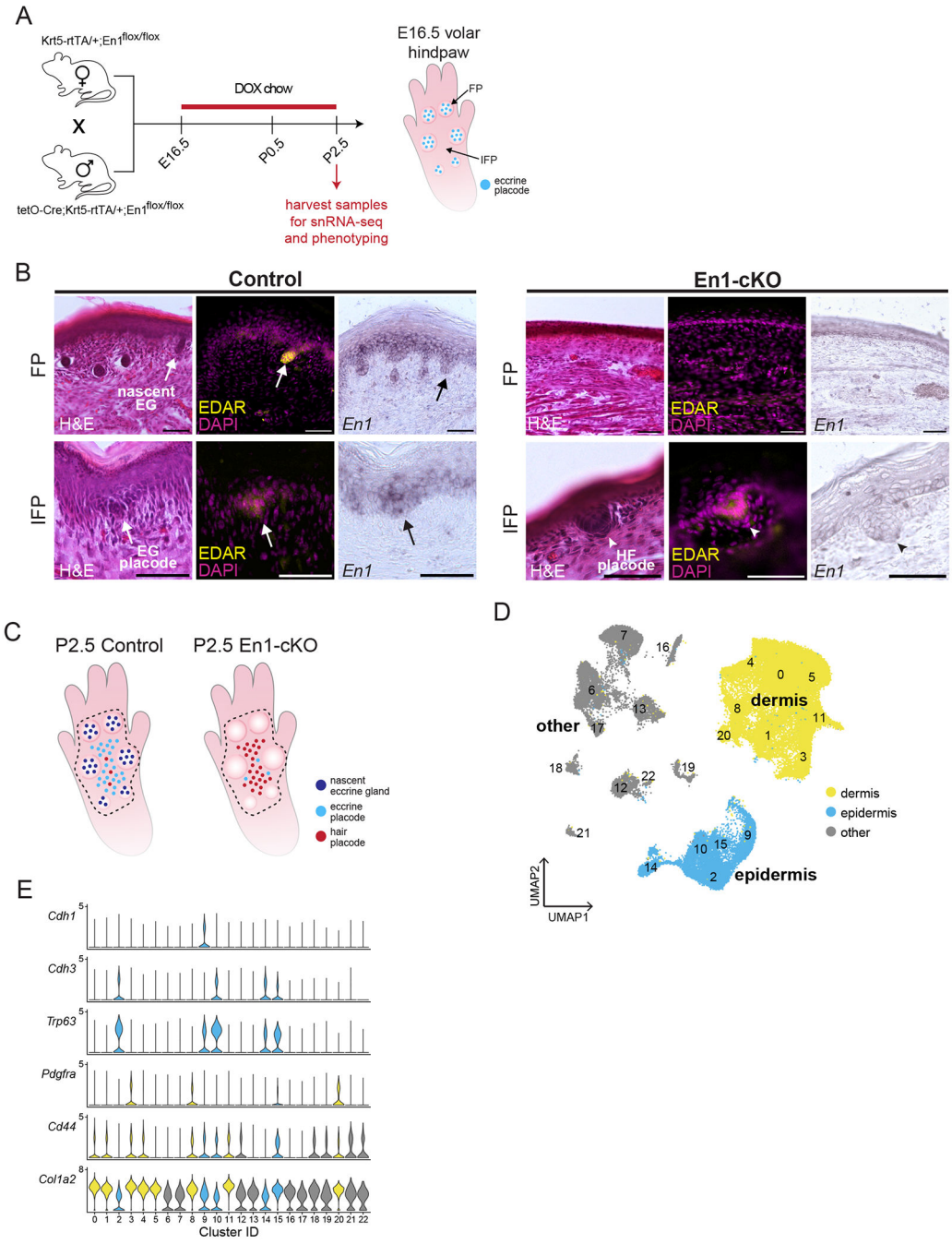

Figure 1. Single nucleus transcriptomic profiling of mouse skin after targeted disruption of eccrine placode identity

A) Mating scheme to generate animals, dosing schedule, and time points for analyses performed in this study. All En1-cKO and Control mice were administered doxycycline (DOX) starting on embryonic day (E)16.5 until day of harvest. Volar hindpaw skin was harvested on post-natal day (P) 2.5 and analyzed as indicated. Schematic of E16.5 volar hindpaw showing appendage composition at start of Dox administration. B) Representative images of stained adjacent sagittal sections through the footpad and interfootpad regions of P2.5 Control (left) and En1-cKO (right) volar skin. First section in series is stained with

Author Manuscript Author Manuscript Author Manuscript Author Manuscript

Hematoxylin and Eosin (H&E) for overall morphology; second section in series is stained with EDAR antibody (yellow) to visualize developing eccrine and hair appendages, as indicated. Section is counterstained with 4′,6-diamidino-2-phenylindole (DAPI; magenta). Hair placode associated dermal condensate (arrowheads). *In situ* hybridization for *En1* (purple) on the third adjacent section in each series. Scale bars represent 50 μm. Eccrine gland (EG), Hair follicle (HF), Footpad (FP), Interfootpad (IFP). C) Schematic of Control (left) and En1-cKO (right) volar hindpaw skin at P2.5 summarizing where nascent glands (dark blue), eccrine placodes (light blue), and hair placodes (red) are found at this stage. Dashed line indicates the region of volar hindpaw skin that was dissected and snap frozen for snRNA-seq. D) UMAP projection of 45,370 nuclei from merged Control and En1-cKO datasets, which were analyzed in this study. Cluster identification numbers are annotated. Epidermal and dermal nuclei are highlighted in blue and yellow, respectively. All other nuclei are in gray. E) Violin plots of gene expression by cluster for markers of the epidermis (*Cdh1, Cdh3, Trp63*) and dermis (*Pdgfra, Cd44, Col1a2*).

Author Manuscript Author Manuscript Author Manuscript Author Manuscript

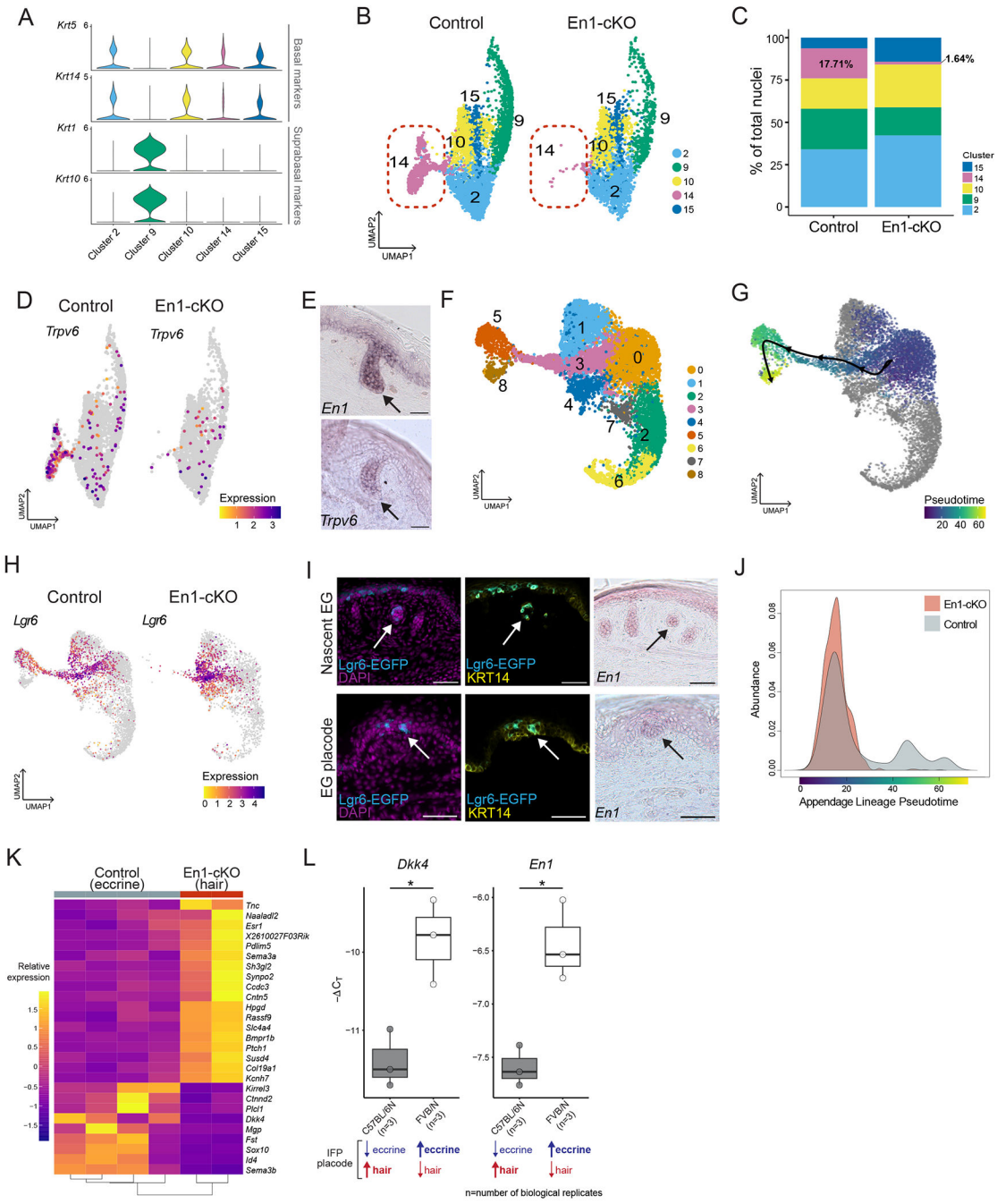

Figure 2. Transitions in the eccrine transcriptome during development

A) Violin plots of gene expression in only epidermal clusters for markers of basal keratinocytes (*Krt5, Krt14*) and suprabasal keratinocytes (*Krt1, Krt10*). B) UMAP projections of epidermal nuclei from original clustering (Figure 1D) colored by cluster identity and split by condition (Control and En1-cKO). Red dashed oval highlights cluster 14, which is depleted in En1-cKO. C) Percent contribution of nuclei from each epidermal cluster to total epidermal nuclei from Control and En1-cKO samples, respectively. Clusters are coded by color as depicted in B. D) Feature plots showing normalized expression of

Author Manuscript Author Manuscript Author Manuscript Author Manuscript

cluster 14 marker *Trpv6* in Control and En1-cKO epidermal nuclei. Negative nuclei are shown in gray. E) *In situ* hybridization for *En1* (top) and *Trpv6* (bottom) in a wildtype footpad at P2.5. Arrow indicates nascent eccrine gland. F) UMAP projection of subclustered epidermal nuclei colored by subcluster identity (merged Control and En1-cKO conditions). G) Results of slingshot trajectory inference mapped onto the subclustered epidermal UMAP embedding that depicts an inferred lineage through epidermal subclusters 0, 3, 5, and 8. Points representing nuclei are colored according pseudotime; nuclei not involved in this lineage are colored gray. H) Feature plot showing normalized expression of *Lgr6*, a top marker of epidermal subcluster 3, for Control (left) and En1-cKO (right) subclustered epidermal nuclei. I) Immunofluorescence staining of sagittal sections through the volar hindlimb skin of Lgr6-EGFP mice at P2.5. Tissue sections are stained with antibodies against EGFP (cyan), which reads out endogenous *Lgr6*, and Keratin 14 (KRT14; yellow) and 4′,6-diamidino-2-phenylindole (DAPI) nuclear stain (magenta). Sections through footpad skin containing nascent eccrine glands (top), and also of the interfootpad region that contains eccrine gland placodes (bottom, arrow) are shown. *In situ* hybridization for *En1* on adjacent serial sections is used to confirm eccrine gland (top and bottom, right). Scale bars represent 50 μm. J) Pseudotime density distribution of Control (gray) and En1-cKO (red) nuclei for slingshot lineage shown in E. Kolmogorov-Smirnov test of the distributions indicates differential progression along this trajectory between the conditions ($p < 2.2e^{-16}$; D = 0.26487). K) Heatmap showing relative expression of transcripts that are differentially expressed between epidermal subcluster 3 nuclei from Control and En1-cKO pseudobulk samples, which are populated by eccrine glands and hair follicles, respectively (p adjusted < 0.01; absolute log2 fold change > 0.58). Columns are pseudobulk sample replicates and rows are genes. L) qRT-PCR results for *Dkk4* (left) and *En1* (right) of volar hindpaw skin from C57BL/6N (n=3 mice) and FVB/N (n=3 mice) mice at P2.5. Each biological sample represents the right and left volar skin from one mouse. Biological samples were assayed in technical quadruplicate. The interfootpad space of C57BL/6N contains mostly hair placodes at P2.5, while that of FVB/N contains mostly eccrine placodes at this stage. Target gene expression is normalized to the reference gene *Rpl13a* and shown as $-\Delta C_T$. Significant differences between groups assessed by Mann-Whitney-Wilcoxon test (* $p < 0.05$).

Author Manuscript
Author Manuscript
Author Manuscript
Author Manuscript

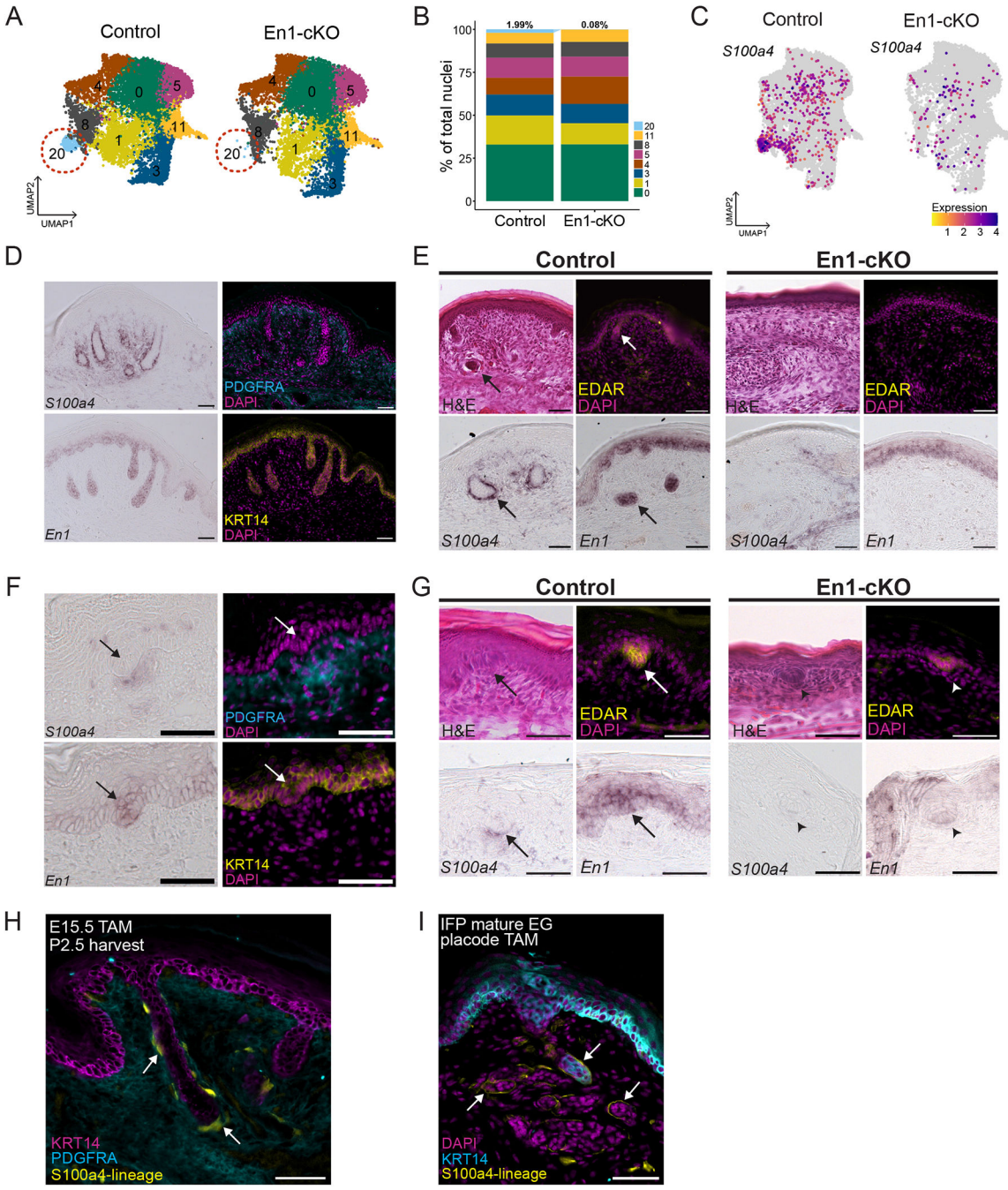

Figure 3. Identification of an *En1*-dependent dermal lineage associated with developing eccrine glands

A) UMAP projections of dermal nuclei colored by cluster identity (original clustering from Figure 1D) and split by condition (Control and En1-cKO). Red, dotted oval highlights cluster 20, which is depleted in En1-cKO. B) Percent contribution of nuclei from each dermal cluster to the total dermal nuclei from Control and En1-cKO samples, respectively. Subclusters are coded by color as depicted in A. C) Feature plots showing relative expression of cluster 20 marker *S100a4*, split by condition. D) *In situ* hybridization for *S100a4* (purple) in sagittal sections of wild type FVB/N P2.5 footpads containing

Author Manuscript Author Manuscript Author Manuscript Author Manuscript

nascent eccrine glands. *En1* expression (purple) by *in situ* hybridization is shown on adjacent sections. Immunofluorescence staining for PDGFRA (cyan), which marks dermal fibroblasts, and KRT14 (yellow), which marks basal keratinocytes. All images shown are from adjacent serial sections. E) Representative images of *in situ* hybridization for *S100a4* (purple) and *En1* (purple) along with EDAR immunofluorescence (yellow) and Hematoxylin and eosin (H&E) staining of adjacent serial sections of control ($En1^{flox/flox}$) and En1-cKO (tetO-Cre; Krt5rtTA/+; $En1^{f/f}$) footpad skin at P2.5. Arrows indicate nascent eccrine glands in the footpad. F) *In situ* hybridization for *S100a4* (purple) in sagittal sections of wild type FVB/N interfootpad skin containing eccrine placodes at P2.5. *En1* expression (purple) shown by *in situ* hybridization on adjacent sections. Immunofluorescence staining for PDGFRA (cyan) marks dermal fibroblasts and KRT14 (yellow) marks basal keratinocytes. All images shown are from adjacent serial sections. Arrows indicate eccrine placodes. G) Representative images of *in situ* hybridization for *S100a4* (purple) and *En1* (purple) along with EDAR immunofluorescence (yellow) and Hematoxylin and eosin (H&E) staining of adjacent serial sections of control ($En1^{flox/flox}$) and En1-cKO (tetO-Cre; Krt5rtTA/+; $En1^{f/f}$) interfootpad skin at P2.5. Arrows indicate eccrine placodes in the interfootpad region. Arrowheads indicate the hair placode and underlying dermal condensate in the interfootpad region of En1-cKO volar skin. H) Fluorescence image of a representative sagittal section through the footpad of a S100a4-CreERT2/+; ROSA-tdTomato/+ mouse at P2.5 that was given tamoxifen at E15.5, around the time of placode formation in the footpads. S100a4-lineage cells are shown in yellow. Immunofluorescence staining for PDGFRA (cyan) marks dermal fibroblasts and KRT14 (magenta) marks basal keratinocytes. I) Fluorescence image of a representative sagittal section through the interfootpad region and mature eccrine gland of an adult S100a4-CreERT2/+;ROSA-mTmG/+ mouse at P22 that was given tamoxifen at P1.5 and P2.5, corresponding to the stage of placode formation in the interfootpad space. S100a4-lineage cells are shown in yellow. Immunofluorescence staining for KRT14 (cyan) marks basal keratinocytes and nuclei are counterstained with DAPI (magenta). Scale bars represent 50 μm (A-I).

Author Manuscript Author Manuscript Author Manuscript Author Manuscript

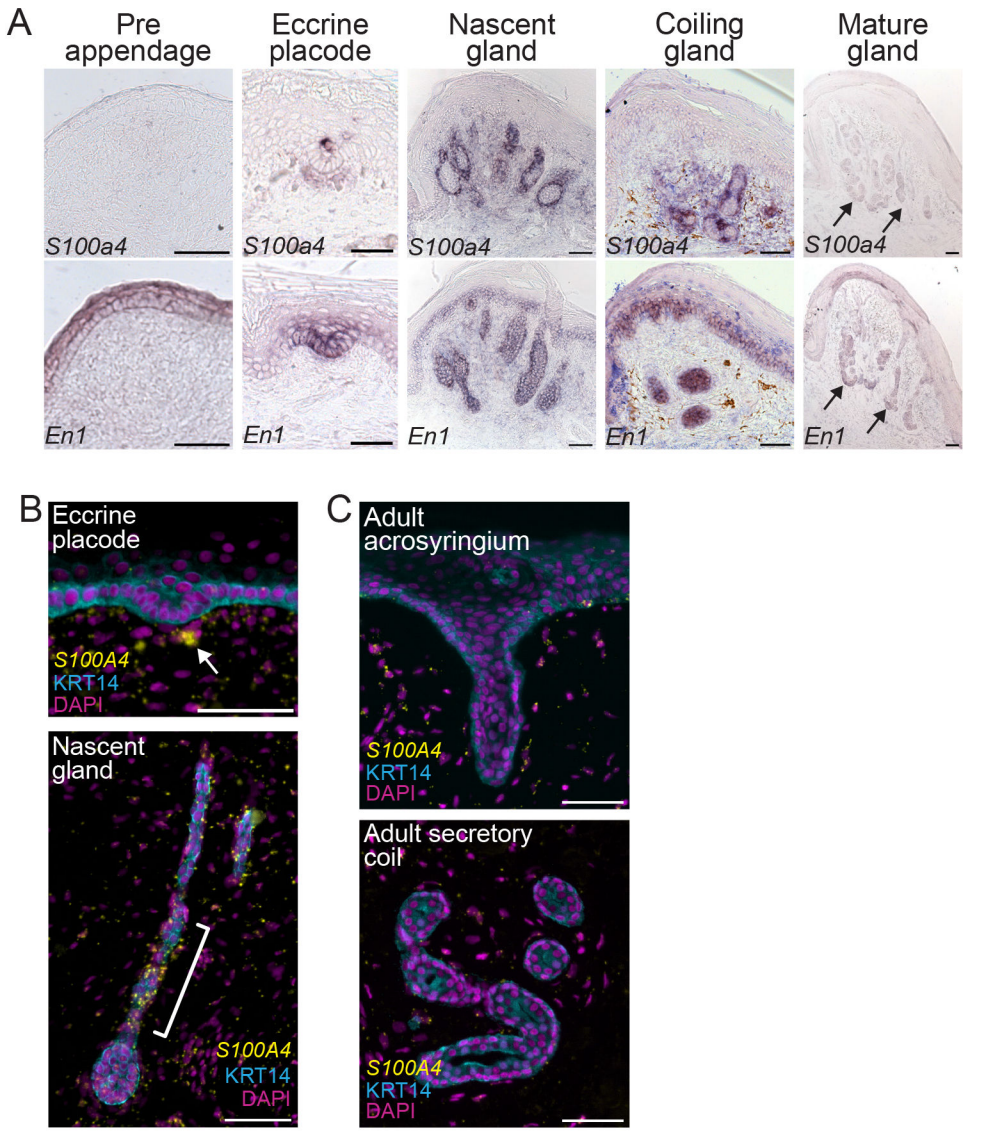

Figure 4. Evolutionary conservation of eccrine-associated dermal population

A) *In situ* hybridization for *S100a4* (top, purple) and *En1* (bottom, purple) in volar skin at distinct stages of eccrine gland development: pre appendage (E15.5; footpad); eccrine placode (P2.5; interfootpad); nascent eccrine gland (P2.5; footpad); coiling eccrine gland (P7; footpad); mature eccrine gland (P28; footpad). B) RNAscope for *S100a4* (yellow) and immunofluorescence for KRT14 (cyan) in developing human plantar skin sections (120 gestational days) containing eccrine placodes (top) and nascent eccrine glands (bottom). C) RNAscope for *S100a4* (yellow) and immunofluorescence for KRT14 (cyan) in adult human cheek skin sections (64 years). Top image shows the apical portion of a mature eccrine gland including the acrosyringium and part of the duct, and bottom image shows the secretory coil from the same gland. Nuclei are counterstained with DAPI (magenta) in fluorescence images (B-C). All scale bars represent 50 μm (A-C).

Author Manuscript Author Manuscript Author Manuscript Author Manuscript

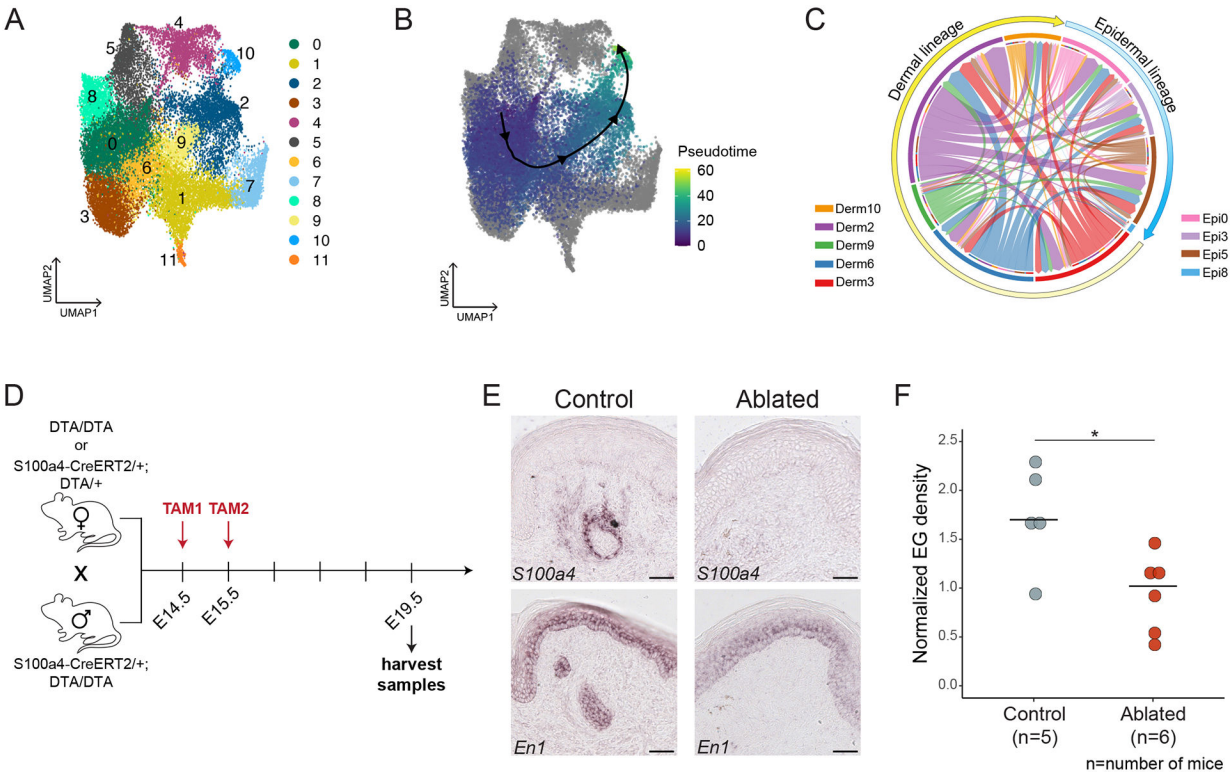

Figure 5. An *En1*-dependent eccrine niche (EDEN) is required for eccrine gland development

A) UMAP projection of subclustered dermal nuclei colored by subcluster identity (merged Control and En1-cKO conditions). B) Results of slingshot trajectory inference mapped onto the subclustered dermal UMAP embedding that depicts an inferred lineage through dermal subclusters 0, 3, 6, 9, 2 and 10. Points representing nuclei are colored according pseudotime; nuclei not involved in this lineage are colored gray. C) Summary chord diagram representing all significant signaling interactions between the dermal and epidermal lineage clusters inferred by CellChat ($p < 0.05$). Clusters are ordered around the circle based on their position in the inferred lineage. D) Experimental scheme for genetic ablation of *En1*-dependent dermal population during eccrine gland development. E) Representative images of *in situ* hybridization for *S100a4* and *En1* from adjacent serial sections of an Ablated sample (S100a4-CreERT2/+;DTA/DTA) compared to a littermate Control (DTA/DTA). F) Quantification of nascent eccrine gland density in the hindlimb footpads of Ablated (n=6 mice) and Control (n=5 mice) mice. Each dot represents the density of eccrine glands in an individual mouse, and one foot was analyzed per mouse. Eccrine gland number for each mouse was normalized to the number of sections scored for the analyzed foot. Cross bars represent sample medians. Significance was assessed by a Mann-Whitney U test (*p = 0.0284; Z = 2.1909; r = 0.66). All scale bars represent 50 μm.

Author Manuscript Author Manuscript Author Manuscript Author Manuscript

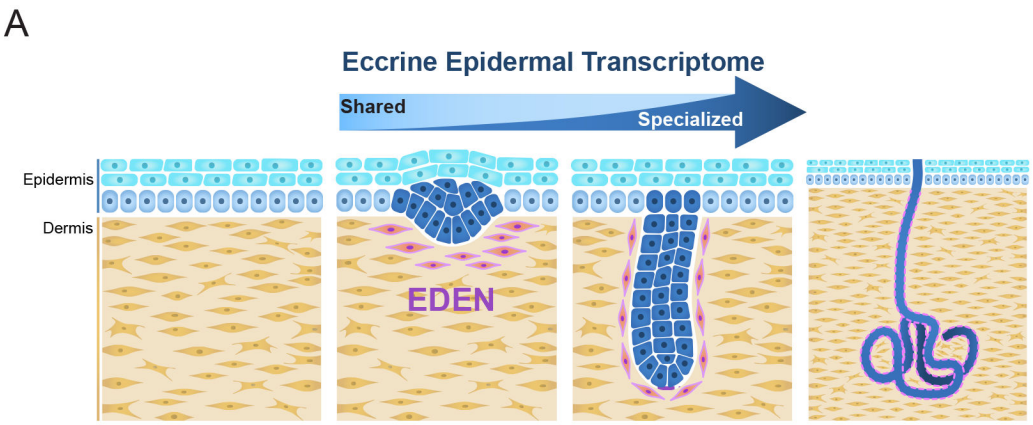

Figure 6. Transcriptional and cellular identifiers of eccrine gland development

A) Model of eccrine gland development incorporating findings reported in this study. Eccrine gland development coordinates a progressive shift in the epidermal transcriptome from one that is predominantly shared with hair follicles, to one that is specialized and eccrine-specific, and requires the *Engrailed 1*-dependent eccrine niche (EDEN; primary niche and its derivative lineage are in pink) within the adjacent dermis. Epidermis is in blue, and dermis exclusive of EDEN is shown in yellow. Pre- and inter-appendage basal keratinocytes are light blue, suprabasal keratinocytes are cyan, and eccrine cells are dark blue. Dermal cells are dark yellow.

Author Manuscript Author Manuscript Author Manuscript Author Manuscript

Key Resource Table

REAGENT or RESOURCE	SOURCE	IDENTIFIER
Antibodies		
Rabbit anti-CK14 (1:10,000)	BioLegends	Cat # 905303
Chick polyclonal anti-GFP (1:1000)	Abcam	Cat# ab13970
Goat polyclonal anti-EDAR (1:100)	R&D Systems	Cat# AF745
Goat polyclonal anti-PDGFRA (1:100)	R&D Systems	Cat# AF1062
Goat polyclonal anti-chicken AF-488 (1:500)	Invitrogen	Cat#A-11039; RRID: AB_2434096
Donkey anti-goat AF-488 (1:200)	Abcam	Cat# ab150129
Donkey anti-rabbit AF-594 (1:250)	Jackson ImmunoResearch	Cat# 711-585-152
Donkey anti-rabbit AF-647 (1:250)	Jackson ImmunoResearch	Cat# 711-605-152
Biological samples		
120 gestational days human plantar foot skin	Birth Defects Research Laboratory, University of Washington (UBMTA: 48286A)	N/A
64 year old human cheek skin	Skin Biology and Disease Resource Center, University of Pennsylvania	N/A
Chemicals, peptides, and recombinant proteins		
Nile Blue A	Sigma-Aldrich	Cat# N5632
Oil Red O	Sigma-Aldrich	Cat# O0625
Dispase II	Sigma-Aldrich	Cat# D4693
4’,6-Diamidino-2-phenylindole	Sigma-Aldrich	Cat# D9542
Critical commercial assays		
NextSeq 500/550 75-cycle High Output v2.5 kit	Illumina	Cat# 20024906
Advantage® UltraPure PCR Deoxynucleotide Mix (10 mM each dNTP)	Clontech	Cat# 639125
Exonuclease I	NEB	Cat# M0293L
NxGen® RNAse Inhibitor	Lucigen	Cat# 30281-2
Maxima H Minus Reverse Transcriptase (200 U/μL)	Life Technologies	Cat# EP0753
KAPA Hifi HotStart ReadyMix	KAPA BioSystems	Cat# KK2602
Barcoded Bead SeqB	ChemGenes	Cat# MACOSKO-2011
Nextera® XT DNA Sample Preparation Kit (96 Samples)	Illumina	Cat# FC-131-1096
Nextera® XT Index Kit (24 indexes, 96 samples)	Illumina	Cat# FC-131-1001
Agilent High Sensitivity DNA Kit	Agilent Technologies	Cat# 5067-4626
Exonuclease I	NEB	Cat# M0293L
QX200™ Droplet Generation Oil for EvaGreen	Bio-Rad	Cat# 1864006
N-Lauroylsarcosine sodium salt solution	Sigma-Aldrich	Cat# L7414-50ML
1H,1H,2H,2H-Perfluoro-1-octanol	Sigma-Aldrich	Cat# 370533-25G
SPRIselect reagent	Beckman Coulter	Cat# B23318

Author Manuscript Author Manuscript Author Manuscript Author Manuscript

REAGENT or RESOURCE	SOURCE	IDENTIFIER
Fluorescent microspheres	Bangs Labs	Cat# FC06F
RNAscope 2.5 HD-RED assay kit	ACD Bio	Cat# 322350
human *S100A4* RNAscope probe	ACD Bio	Cat# 422071
human *PPIB* RNAscope probe	ACB Bio	Cat# 313901
DapB negative control RNAscope probe	ACD Bio	Cat# 310043
Deposited data		
Raw and processed snRNA-seq data	This paper	GEO: GSE220977
Experimental models: Organisms/strains		
Mouse: tetO-Cre: *Tg(tetO-cre)1Jaw/J*	The Jackson Laboratory; Perl et al. 2002[32]	RRID: ISMR_JAX:006224
Mouse: Krt5-rtTA: *Tg(KRT5-rtTA)T2D6Sgkd/J*	Laboratory of Dr. Sarah Millar (Icahn School of Medicine at Mt. Sinai); Diamond et al. 2000[33]	RRID: ISMR_JAX:017519
Mouse: En1^{flox}: *En1tm8.1Alj/J*	Laboratory of Dr. Alexandra Joyner (Memorial Sloan Kettering Cancer Center); Sgaier et al. 2007[31]	RRID: ISMR_JAX:007918
Mouse: Lgr6-eGFP: *Lgr6tm2.1$^{(cre/ERT2)Cle}$/J*	Laboratory of Dr. Pantelis Rompolas (University of Pennsylvania); Snippert et al. 2010[62]	RRID: ISMR_JAX:016934
Mouse: S100a4-CreERT2: S100a4-T2A$^{(CreERT2)}$	Dr. Mayumi Ito (New York University)	N/A
Mouse: ROSA-DTA: Gt(ROSA)26Sor$^{tm1(DTA)Lky}$/J	The Jackson Laboratory; Voehringer et al. 2008[48]	RRID: ISMR_JAX:009669
Mouse: mTmG: Gt(ROSA)26Sor$^{tm4(ACTB-tdTomato,-EGFP)Luo}$/J	Laboratory of Dr. George Cotsarelis (University of Pennsylvania); Muzumdar et al. 2007[64]	RRID: IMSR_JAX:007576
Mouse: ROSA-tdTomato: *Gt(ROSA)26Sor$^{tm14(CAG-tdTomato)Hze}$*/J	Laboratory of Dr. Pantelis Rompolas (University of Pennsylvania); Madisen et al. 2010[63]	RRID: IMSR_JAX:007914
Oligonucleotides		
Primers for amplifying cDNA to make *in situ* hybridization probes, see Table S4	This paper	N/A
Primers for mice, see Table S4	This paper	N/A
Primers for qRT-PCR, see Table S4	This paper	N/A
Software and algorithms		
FIJI	Schindelin et al. 2012[65] (doi: 10.1038/nmeth.2019)	N/A
Drop-seq Tools v1.12	Macosko et al. 2015[66] (doi: 10.1016/j.cell.2015.05.002)	N/A
Seurat v4.0.2	Hao, Hao, et al. 2021[67] (doi: 10.1016/j.cell.2021.04.048)	N/A
Harmony	Korsunsky et al. 2019[37] (doi: 10.1038/s41592-019-0619-0)	N/A
Slingshot	Street et al. 2018[70] (doi: 10.1186/s12864-018-4772-0)	N/A
DESeq2	Love et al. 2014[69] (doi: 10.1186/s13059-014-0550-8)	N/A

Author Manuscript Author Manuscript Author Manuscript Author Manuscript

REAGENT or RESOURCE	SOURCE	IDENTIFIER
ClusterProfiler	Wu et al. 2021[68] (doi: 10.1016/j.xinn.2021.100141)	N/A
CellChat	Jin et al. 2021[47] (doi: https://doi.org/10.1038/s41467-021-21246-9)	N/A
Other		
Leica M680 microscope	Leica	N/A
Leica IC90E camera	Leica	N/A
Leica DM5500B microscope	Leica	N/A
Leica DFC 500 camera	Leica	N/A
Leica DFC 360X camera	Leica	N/A
Qubit 3.0	Invitrogen	N/A
Applied Biosystems QuantStudio 7 Flex real-time PCR machine	ThermoFisher Scientific	REF# 4485701
Bioanalyzer	Agilent	N/A
Illumina NextSeq 500	Illumina	N/A
Dox Diet, Grain-Based, Doxycycline (6 gm/kg), Green, 1/2” Pellets Gamma irradiated	Bio-Serv	Cat# S4096
PDMS co-flow microfluidic droplet generation device	uFluidix	N/A